Cosmogenic 3He chronology of postglacial lava flows at Mt Ruapehu, Aotearoa / New Zealand

Pedro Doll, Shaun Robert Eaves, Ben Matthew Kennedy, Pierre-Henri Blard, Alexander Robert Lee Nichols, Graham Sloan Leonard, Dougal Bruce Townsend, Jim William Cole, Chris Edward Conway, Sacha Baldwin, et al.

Geochronology, 6, 365–395, 2024
https://doi.org/10.5194/gchron-6-365-2024

Cosmogenic ^{3}He chronology of postglacial lava flows at Mt Ruapehu, Aotearoa / New Zealand

Pedro Doll[1], Shaun Robert Eaves[2,3], Ben Matthew Kennedy[1], Pierre-Henri Blard[4], Alexander Robert Lee Nichols[1], Graham Sloan Leonard[5], Dougal Bruce Townsend[5], Jim William Cole[1], Chris Edward Conway[6], Sacha Baldwin[1,★], Gabriel Fénisse[4,★], Laurent Zimmermann[4,★], and Bouchaïb Tibari[4,★]

[1]School of Earth and Environment, University of Canterbury, Private Bag 4800, Ōtautahi / Christchurch 8041, New Zealand
[2]Antarctic Research Centre, Victoria University of Wellington, P.O.Box 600, Te Whanganui-a-Tara / Wellington 6140, New Zealand
[3]School of Geography, Environment and Earth Sciences, Victoria University of Wellington, P.O. Box 600, Te Whanganui-a-Tara / Wellington 6140, New Zealand
[4]CRPG, CNRS, Université de Lorraine, 15 Rue Notre Dame des Pauvres, Vandoeuvre-les Nancy 54000, France
[5]GNS Science, 1 Fairway Drive, Avalon, Te Awa Kairangi ki Tai / Lower Hutt 5011, New Zealand
[6]Geological Survey of Japan, National Institute of Advanced Industrial Science and Technology (AIST), 1-1-1 Higashi, Tsukuba, Ibaraki 305-8567, Japan
★These authors contributed equally to this work.

Correspondence: Pedro Doll (pedro.doll@pg.canterbury.ac.nz)

Received: 18 January 2024 – Discussion started: 23 January 2024
Revised: 31 March 2024 – Accepted: 10 May 2024 – Published: 10 July 2024

Abstract. Accurate volcanic hazard assessments rely on a detailed understanding of the timing of past eruptions. While radiometric methods like ^{40}Ar/^{39}Ar or K/Ar are by far the most conventional lava flow dating tools, their low resolution for young (< 20 ka) deposits interferes with the development of precise chronologies of recent effusive activity on most volcanoes. Mt Ruapehu (Aotearoa / New Zealand) has produced many lava flows throughout its history, but the precise timing of many recent eruptions remains largely unknown. In this study, we use cosmogenic ^{3}He exposure dating to provide 23 eruption ages of young lava flows at Ruapehu. We then compare our results with existing ^{40}Ar/^{39}Ar and paleomagnetic constraints, highlighting the value of cosmogenic nuclide exposure dating in refining recent eruptive chronologies. Of the 23 sampled flows, 16 provided robust eruption ages (5 %–20 % internal 2σ; $n \geq 3$) between ca. 20 and 8 ka, except for one lava flow that erupted at around 43 ka, and their age distribution indicates that, during the last 20 kyr, effusive activity at Ruapehu peaked at 17–12 ka and at 9–7.5 ka. Nearly identical eruption ages of lavas located in different flanks of the volcanic edifice suggest concurrent activity from multiple vents during relatively short time intervals (0–2 kyr) at around 13, 10, and 8 ka. We analysed four individual lava flows previously dated by ^{40}Ar/^{39}Ar, two of which yield eruption ages older than the older limit of the 2σ interval of the radiometric dates, but the good clustering of individual samples from our sites suggests that our results better represent the real eruption age of these flows. Our ^{3}He-based chronology shows excellent agreement with paleomagnetic constraints, suggesting that production rate uncertainties are unlikely to impact the accuracy of our eruption ages. This study demonstrates how cosmogenic nuclide dating can provide greater detail on the recent effusive chronology of stratovolcanoes, helping to resolve the low resolution of and difficulty in applying radiometric dating methods to young lava flows.

1 Introduction

Effusive volcanism is the main mechanism driving edifice growth on stratovolcanoes and poses a great hazard to the infrastructure, the natural environment, and the social fabric

and livelihoods of local communities (Trusdell, 1995; Wilson et al., 2014; Harris, 2015; Jenkins et al., 2017; Tsang and Lindsay, 2020). Accurate hazard assessments rely on precise knowledge of recent eruption footprints, magnitudes, and frequencies (Connor et al., 2015) and, hence, accurate dating of eruptive events.

Most chronological studies of lava flows on stratovolcanoes are based on radiometric methods such as ^{40}Ar/^{39}Ar and K/Ar. Recent advances in these methods (Coble et al., 2011; Fleck et al., 2014; Clay et al., 2015) have improved the precision of age determinations for Pleistocene lavas. However, errors in the ages of young (< 20 ka) products are still too large to precisely resolve recent eruptive chronologies (e.g. Wijbrans et al., 2011; Conway et al., 2016; Ramos et al., 2016; Calvert et al., 2018; Preece et al., 2018; Pure et al., 2020), hindering our ability to discriminate distinct eruptive episodes or to determine temporal relationships between effusive eruptions and other volcanic processes. If available, radiocarbon dating of burned coal beneath lava flows can provide accurate eruption ages, and it has been used widely in Hawai'i (e.g. Buchanan-Banks et al., 1989; Trusdell, 1995; see also Lockwood and Lipman, 1980) as well as in various volcanic regions (e.g. Moore and Rubin, 1991; Mishra et al., 2019; Sherrod et al., 2006). However, the use of radiocarbon is limited to areas with sufficient vegetation at the time of lava flow emplacement, so it is not applicable at high elevations or in periglacial environments. Alternative methods, such as paleomagnetism or cosmogenic nuclide exposure dating, can support radiometric studies in non-vegetated areas and considerably reduce ^{40}Ar/^{39}Ar and K/Ar uncertainties for Late Pleistocene and Holocene products (Sherrod et al., 2006; Parmelee et al., 2015; Wright et al., 2015; Greve et al., 2016) and are therefore important when generating more accurate eruptive histories in a wider spectrum of volcanic environments.

Cosmogenic nuclides are isotopes that originate when primary and secondary cosmic rays interact with atomic nuclei (Leya et al., 2000; Dunai, 2010). Some of them (terrestrial in situ cosmogenic nuclides, or TCNs) are formed in the upper few metres of the Earth's surface and can be used to calculate exposure ages of geological deposits provided they are rare in geological materials, are produced and retained in common minerals, are able to be analysed with reasonable confidence, are stable or have a half-life comparable to the timescales of the studied process, and have a well-understood origin and known relative contributions of their production mechanisms (Dunai, 2010). The number of TCNs that fulfil these requirements and have well-established methodologies developed for Earth science applications is relatively small (see Dunai, 2010), and the production rates and retention efficiency of TCNs vary across different minerals. ^{3}He is a stable isotope with the highest production rate of all TCNs and a low detection limit in several geological settings (Blard, 2021), which makes it the ideal nuclide for dating young lava flows (Gosse and Phillips, 2001). This gas suffers diffusion loss in felsic minerals (e.g. quartz and feldspars, and in volcanic groundmass containing them; Lippolt and Weigel, 1988; Tremblay et al., 2014) at Earth's surface temperatures, and it is therefore not normally used for silicic lithologies, which are better studied using ^{10}Be or ^{26}Al (e.g. Klein et al., 1986; Nishiizumi et al., 1991; Smith et al., 2005). ^{3}He is more efficiently retained in olivines and pyroxenes (Kurz, 1986a; Gosse and Phillips, 2001; Shuster et al., 2004; Blard, 2021), so it is suitable for dating volcanic eruptions (e.g. Kurz et al., 1990; Foeken et al., 2009; Parmelee et al., 2015), reconstructing glacial histories (e.g. Cerling and Craig, 1994; Blard et al., 2007) and fault kinematics (e.g. Fenton et al., 2001), or estimating erosion rates (e.g. Ferrier et al., 2013; Puchol et al., 2017), considering that the studied rocks contain these minerals.

Surface exposure dating using TCNs is applicable to geological deposits that have been brought to the surface and remained exposed to the cosmic ray flux ever since, provided there is no significant erosion or shielding (glacial, snow, debris, soil, tephra, or vegetation cover) that could have affected their cosmogenic nuclide inventory. In temperate climates, suitable sites will lie at elevations between the vegetation limit and where cryogenic processes begin to dominate. In dynamic environments such as stratovolcanoes, original surfaces are more likely to be preserved on younger lava flows, which have had a relatively limited time exposed to erosive and/or depositional processes. In addition, flow interiors with crystalline groundmass necessary for ^{40}Ar/^{39}Ar or K/Ar dating are less likely to be exposed in young lava flows for the same reason. For young lava flows, cosmogenic ^{3}He (^{3}He$_{cos}$) has the potential to resolve events down to 100 years under the most favourable conditions (low magmatic He and eruption ages ≤ 10 ka; Niedermann, 2002) and commonly yields ages with uncertainties of 15 %–20 % (2σ including production rate errors), which is significantly more precise than traditional radiometric techniques for lavas < 20 ka (e.g. Wijbrans et al., 2011; Calvert et al., 2018; Pure et al., 2020). Thus, ^{3}He$_{cos}$ can be used to complement chronological studies by providing greater detail of recent construction histories of volcanic edifices (e.g. Kurz et al., 1990; Foeken et al., 2009; Espanon et al., 2014; Parmelee et al., 2015). However, most of this research is focused on basaltic lava flows in extensional environments (e.g. Kurz et al., 1990; Licciardi et al., 2007; Foeken et al., 2009; Espanon et al., 2014; Marchetti et al., 2014; Medynski et al., 2015), and the application of ^{3}He$_{cos}$ on stratovolcanoes (e.g. Parmelee et al., 2015) is still limited. 'A'ā lavas (commonly found in andesitic stratovolcanoes) normally have prominent tumuli standing out from the landscape, which are less likely to accumulate large amounts of snow or tephra compared to flatter primary morphologies (e.g. ropy pāhoehoe surfaces targeted in basic lavas; Kurz et al., 1990; Espanon et al., 2014; Marchetti et al., 2014; Parmelee et al., 2015), making them ideal targets for surface exposure dating (see Licciardi et al., 2007).

In this paper, we use surface exposure dating with terrestrial in situ $^{3}He_{cos}$ in pyroxenes and olivines to provide 23 eruption ages of mainly postglacial (< 20 ka) lava flows at Mt Ruapehu, a large (summit 2797 m a.s.l.) andesitic stratovolcano located in the centre of Te Ika-a-Māui / North Island of Aotearoa / New Zealand). We then compare our results with previous $^{40}Ar/^{39}Ar$ and paleomagnetically refined ages as well as with eruption age assumptions based on geochemical fingerprinting, and we test the applicability of $^{3}He_{cos}$ as a lava flow dating tool for stratovolcanoes, showcasing the method's capacity to provide high-resolution ages for young lava flows and to identify distinct eruptive episodes in short time intervals.

2 Geological background

2.1 Study area

Ruapehu is a cultural and spiritually significant *Maunga* (Māori word for mountain) for the local iwi (Māori word for *tribe*) Ngāti Rangi, Ngāti Tūwharetoa, and Uenuku (see Gabrielsen et al., 2018). This volcano is the southernmost continental expression of the Taupō Volcanic Zone (TVZ, Fig. 1) related to the Hikurangi Trench, which is located at the southern end of the Tonga–Kermadec arc subduction system (Cole and Lewis, 1981). The TVZ can be divided into three segments: the northern, central, and southern TVZ (Fig. 1a), distinguished by composition and eruptive styles. The northern TVZ has several andesitic stratovolcanoes, including Whakaari / White Island and Motuhara off the northeastern coast of Te Ika-a-Māui / North Island. The central TVZ is one of the most productive silicic volcanic systems in the world, with at least 34 caldera-forming events in the last 1.6 Myr, including Taupō and Ōkataina (Houghton et al., 1995; Wilson et al., 2009). The southern zone is dominated by the andesitic stratovolcanoes Tongariro and Ruapehu with subordinate basalts (e.g. Ohakune Formation basalt).

Ruapehu is the largest and one of the most active stratovolcanoes in mainland Aotearoa / New Zealand (Leonard et al., 2021). The current edifice is mostly formed by pyroxene-bearing basaltic andesite, andesite, and dacite lavas, which erupted throughout four main constructive periods and are encompassed in distinct units: Te Herenga (200–150 ka), Waihianoa (150–80 ka), Mangawhero (50–15 ka), and Whakapapa (15–2 ka) formations (Hackett, 1985; Townsend et al., 2017, Table 1). Contemporary to lava flow emplacement, Ruapehu generated many explosive eruptions (Topping and Kohn, 1973; Donoghue et al., 1995; Pardo et al., 2012a), including several Plinian events (Pardo, 2012) preserved as tephra sequences on the eastern volcanic ring plain, although the timing of these eruptions is not well constrained. In this study, we focus on the Whakapapa Formation and the youngest member of the Mangawhero Formation (Fig. 1; Table 1), providing greater detail of the recent effusive activity of Ruapehu.

Eruption ages of Ruapehu's lava flows were first determined using K/Ar (Stipp, 1968; Tanaka et al., 1997) and later improved with $^{40}Ar/^{39}Ar$ by Gamble et al. (2003) and Conway et al. (2016). Combining these $^{40}Ar/^{39}Ar$ ages with an extensive geochemical survey, Conway et al. (2016) divided lavas from the Mangawhero and Whakapapa formations into distinctive packages, later formalized as members by Townsend et al. (2017, Table 1). However, many lava flows are only assumed to have been erupted in specific time periods due to their geochemical similarity and/or geographical proximity to flows with geochronological constraints.

Throughout its history, Ruapehu has periodically been covered by glaciers controlling lava flow emplacement (Conway et al., 2015). The edifice displays characteristic erosional and depositional glacial landforms extending from current glaciers down to ∼ 1200 m a.s.l. (Mc Arthur and Shepherd, 1990; Eaves et al., 2016a; Townsend et al., 2017) and conspicuous large-scale and fine-scale features indicative of lava–ice interaction. During heavily glaciated periods, lava emplacement and preservation were restricted to inter-valley ridges, and cooling against ice generated overthickened lava margins (ice-bounded flows; Conway et al., 2015) still visible in the landscape. Based on the distribution of these ice-bounded lava flows, Conway et al. (2016) suggested a peak in glacial expansion between 42 and 31 ka and a reduction in ice thickness between 31 ka and the last stages of the Last Glacial Maximum (LGM) at 20–15 ka (Barrell et al., 2013), prior to the glacial retreat. Effusive deposits that erupted after the LGM (postglacial lavas of the Whakapapa Formation, Fig. 1) were free to flow to the valley floors and finish shaping the modern landscape observed at Ruapehu. Eaves et al. (2019) provided $^{3}He_{cos}$ ages for moraine groups in the Mangaehuehu valley (south Ruapehu), recording pulsatory glacial retreat after the LGM. Based on $^{3}He_{cos}$ exposure ages of boulders, they proposed moraine construction periods and associated equilibrium line altitudes of 2100 m a.s.l. at ∼ 14–11 ka, 2250 m a.s.l. at 4.5 ka, and 2300 m a.s.l. 200–500 years ago. Present glaciers on Ruapehu (3.0 km^2 in 2016; Eaves and Brook, 2021) are restricted to some upper catchment areas over 2250 m a.s.l., the largest of which is located on its summit plateau at > 2500 m a.s.l.

2.2 Previous chronological studies on postglacial lavas

The first constraints on eruption ages of Whakapapa lavas were given from studies of tephra layers (Topping, 1974; Price et al., 2012). Conway et al. (2016) were the first to provide absolute ages using $^{40}Ar/^{39}Ar$, for which samples from slowly cooled lava interiors are needed, as Ar analyses are done in crystalline groundmass (glass contents < 5 %) with large microlites. The lack of abundant exposures of lava interiors limited its application to only 10 flows, and, although this technique yielded reasonably precise ages for lavas > 20 ka, their relative errors increase with decreasing

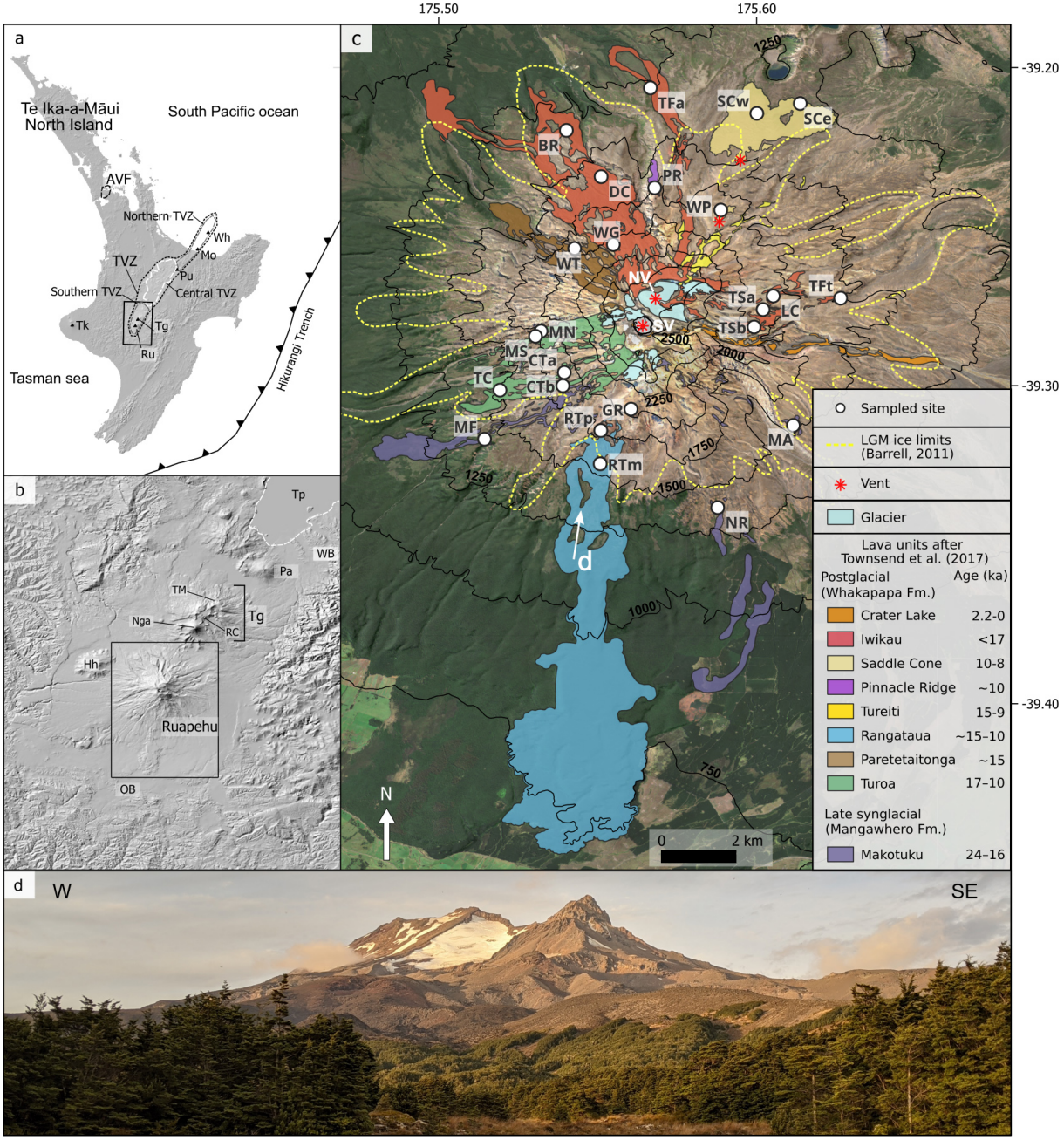

Figure 1. Location map of study area. **(a)** Te Ika-a-Māui / North Island (Aotearoa / New Zealand) with its main active volcanic areas detailed: AVF – monogenetic Auckland Volcanic Field, Wh – Whakaari / White Island, Mo – Motuhara, Pu – Putauaki, TVZ – Taupō Volcanic Zone, Tg – Tongariro, Ru – Ruapehu, and Tk – Taranaki. **(b)** Detail of the "Central Plateau" at the southern end of the TVZ: Tp – Taupō, WB – Waimarino basalt, Pa – Pihanga , Tg – Tongariro, TM – Te Maari, Nga – Ngauruhoe, RC – Red Crater, Hh – Hauhungatahi, and OB – Ohakune Formation basalt. **(c)** Study area, with Ruapehu's postglacial and late synglacial lava units mapped after Townsend et al. (2017), and sampled sites in this study. The maximum glacial extent during the LGM (Last Glacial Maximum; ~ 20–15 ka) after Barrell (2011) is outlined by the dashed yellow line. Panel **(c)** shows the NV – northern vent and SV – southern vent. Abbreviations next to sampled sites refer to lava flow names; there is a full list in Table A1. **(d)** Photo of Ruapehu taken from the south, with the Mangaehuehu Glacier directly beneath Ruapehu's summit (viewpoint's location is shown in panel **(c)** with the white arrow labelled as "d").

Table 1. Previous chronological studies from lava flows at Ruapehu.

Formation	Member		Eruption ages ($\pm 2\sigma$)	Methods	^{3}He-based eruption ages, this study (ka, $\pm 2\sigma$)
Whakapapa (< 15 ka; postglacial)	Crater Lake (< 5 ka)		2400–2050 BP[a], 0.2 ± 2.2 ka[b]	Paleomagnetism (refined from ^{40}Ar/^{39}Ar)	–
	Iwikau	Tawhainui flows (9–7 ka)	DC: 8200–7900 BP[a], 6.0 ± 2.4 ka[b]; BR: 8800–8500 BP[a]	Paleomagnetism (refined from ^{40}Ar/^{39}Ar and tephra stratigraphy)	DC: 7.8 ± 1.5; BR: 8.1 ± 2.1; WG: ≥7.8 ± 2.4
		Mangatoetoenui flows (< 17 ka*)	LC: 0.8 ± 5.6 ka; TSb: 9.2 ± 8.0 ka[b]	^{40}Ar/^{39}Ar	LC: 11.4 ± 2.3; TSa: 9.4 ± 1.8; TSb: 11.5 ± 2.2; TFt: ≥8.6 ± 2.6
		Taranaki Falls flow (11–9 ka*)	TFa: 10 800–8900 BP[a], 8.8 ± 2.8 ka[b]	Paleomagnetism (refined from ^{40}Ar/^{39}Ar)	TFa: 14.6 ± 2.9
	Saddle Cone (10–8 ka*)		SC: 9850–8650 BP[a]	Paleomagnetism (refined from tephra stratigraphy)	SC: 9.9 ± 2.0; WP: ≥11.2 ± 2.2
	Pinnacle Ridge (~ 10 ka*)		PR: ~ 10 ka[c]	Correlation with tephra	PR: 20.4 ± 4.0
	Tureiti (15–9 ka)		12.5 ± 2.6; 11.9 ± 2.8 ka[b]	^{40}Ar/^{39}Ar	–
	Rangataua (~ 15–10 ka*)		~ 15–10 ka[d,e]	Stratigraphy	RTp: 13.6 ± 2.6; RTm: 15.8 ± 3.0
	Paretetaitonga (~ 15 ka)		14.8 ± 3.0 ka[b]	^{40}Ar/^{39}Ar	WT: 13.3 ± 2.6
	Turoa (17–10 ka*)		15.1 ± 2.4; 11.9 ± 2.2 ka[b]	^{40}Ar/^{39}Ar	MN: 8.3 ± 1.6; MS: ≥6.1 ± 1.7; CTa: ≥13.6 ± 2.7; CTb: 8.6 ± 1.7; TC: 13.4 ± 2.6
Mangawhero (50–15 ka; synglacial)	Makotuku (24–16 ka)		20.9 ± 2.8; 17.8 ± 2.2 ka[b]	^{40}Ar/^{39}Ar	MF: 12.6 ± 3.5; NR: 42.9 ± 8.6; MA: ≥54.0 ± 18.0
	Waitonga (25–21 ka)		23.0 ± 1.6[b]; 23 ± 8 ka[f]	^{40}Ar/^{39}Ar	–
	Te Piripiri (~ 21 ka)		21 ± 6 ka[f]	^{40}Ar/^{39}Ar	–
	Horonuku (29–15 ka)		23 ± 4; 22 ± 7 ka[f]	^{40}Ar/^{39}Ar	–
	Whakapapaiti (~ 26 ka)		25.7 ± 3.8 ka[b]	^{40}Ar/^{39}Ar	–
	Manganuioteao (36–22 ka)		25.7 ± 2.6; 27.2 ± 4.8; 30.7 ± 5.2; 30.9 ± 2.2 ka[b]	^{40}Ar/^{39}Ar	–
	Mananui (42–38 ka)		40.3 ± 2.2[b]	^{40}Ar/^{39}Ar	–
	Te Kohatu (44–36 ka)		47.6 ± 1.4; 39.1 ± 1.4; 39.2 ± 2.0; 42.6 ± 1.8 ka[b]	^{40}Ar/^{39}Ar	–
	Mangaturuturu (46–36 ka)		38.4 ± 2.4; 41.3 ± 1.8; 43.4 ± 2.4 ka[b]	^{40}Ar/^{39}Ar	–
	Mangaehuehu (47–40 ka)		42.8 ± 1.0; 43.1 ± 1.4; 43.3 ± 1.6; 44.2 ± 1.8; 45.4 ± 2.0 ka[b]	^{40}Ar/^{39}Ar	GR: ≥14.2 ± 2.7
	Ngahuinga (48–35 ka)		44.8 ± 3.0 ka[b]	^{40}Ar/^{39}Ar	–
Waihianoa (166–80 ka)			88.1 ± 6.4; 95.9 ± 7.0; 120.7 ± 4.0; 121.4 ± 2.8; 121.7 ± 4.2; 133.6 ± 6.4[b]; 119 ± 12; 129 ± 15; 130 ± 23; 131 ± 27; 133 ± 11; 134 ± 12; 135 ± 14; 138 ± 14; 147 ± 10; 147± 12; 154 ± 12 ka[f]	^{40}Ar/^{39}Ar	–
Te Herenga (200–150 ka)			158.8 ± 8.2; 169.4 ± 7.8; 174.6 ± 3.4 186.2 ± 6.8; 187.9 ± 34.4[b]; 183 ± 13; 197 ± 12; 205 ± 27 ka[f]	^{40}Ar/^{39}Ar	–

[a] Greve et al. (2016). [b] Conway et al. (2016). [c] Donoghue et al. (1999). [d] Price et al. (2012). [e] Eaves et al. (2016b). [f] Gamble et al. (2003). * Age limits redefined in this study based on $^{3}He_{cos}$ eruption ages. Ages separated by commas represent the same lava flow and semicolons separate dates from different flows.

age, varying between 16 % and 23 % for 20–11 ka deposits and 32 % and 1000 % for Holocene lavas (see Table 1).

Greve et al. (2016) refined the eruption age for ^{40}Ar/^{39}Ar-dated and tephra-constrained Holocene lava flows by comparing characteristic magnetization directions recorded in the lavas with a paleosecular variation record based on lake sediments from Mavora Lakes (Te Waipounamu / South Island, Aotearoa / New Zealand), which were independently calibrated using ^{14}C (Turner et al., 2015). Dating lava flows using paleomagnetic directions, however, requires a previous eruption age constraint and is limited to the Holocene in Aotearoa / New Zealand due to the extension of the sediment record. Only the ages of five flows were constrained using this method: one from the Crater Lake Member, three from the Iwikau Member (Delta Corner, Bruce Road, and Taranaki Falls flows), and one from the western lobe of the Saddle Cone Member. Eruption ages provided by Greve et al. (2016) for the Crater Lake, Delta Corner, and Bruce Road flows are tightly constrained (age ranges of ca. 300 years), while the preferred ages for the Taranaki Falls flow and Saddle Cone Member span ∼ 2 and ∼ 1.2 kyr, respectively (Table 1).

3 Methods

3.1 Sampling site selection

The selection of an adequate sampling site is an important step for cosmogenic nuclide exposure dating. Evidence of negligible erosion and confidence that the targeted rock has not been covered by other rocks, soil, ice, volcanic ash, or vegetation for a significant amount of time since formation are essential. For lava flows, effective sampling was achieved by targeting tumuli, spikes, and other features standing above the main flow surface (e.g. Anderson et al., 1994; Licciardi et al., 2006), which preserve characteristic primary cooling morphologies of flow surfaces (Fig. 2). Additional photos of sampled sites and examples of sites that are not suitable can be found in the Supplement file S1.

Using aerial photographs and digital elevation models (DEMs) based on aerial imagery and a newly acquired lidar dataset, we revised the existing maps (Townsend et al., 2017) and identified individual lava flows within each of the different members of the Whakapapa Formation, which we then targeted in our sampling. Lack of adequate lava surface exposures did not permit us to sample lavas from the Tureiti and Crater Lake members. Due to the lack of chronological data of several lavas of the Makotuku Member of the Mangawhero Formation (24–16 ka; Conway et al., 2016, Table 1), we additionally targeted three flows of this unit on outcrops outside of the LGM ice limits (MF, NR, and MA; Fig. 1c). We also sampled a site (GR) that we consider to be postglacial due to the presence of original (non-eroded) lava surfaces and its location inside the LGM ice limit of Barrell (2011, Fig. 1c). Note that this exposure was previously mapped as the Mangawhero Formation (Mangaehuehu Member) based primarily on its location on the volcano and similarity in appearance to nearby geochemically fingerprinted outcrops.

3.2 Sample collection

All samples were collected under a research and collection permit of the Department of Conservation of Aotearoa / New Zealand, which was obtained after a consultation process involving local iwi with rightful claims to guardianship of Ruapehu. We sampled between three and six shallow surfaces (< 6 cm below the flow top) for each targeted flow using a hammer and chisel. For recording the coordinates and altitude of each surface, we used a differential Trimble Geo 7X GPS (vertical precision of 0.1 m) corrected by data of VGMT (Ohakune, Land Information New Zealand) and the Chateau Observatory base (GeoNet) stations. We also measured surface dip and orientation and azimuth–horizon angle pairs to account for topographic shielding. For the CTa, CTb, and TC samples, in situ topographic shielding could not be acquired, so representative azimuth–horizon angle pairs were selected based on observations of DEMs. To test the accuracy of this approach, we compared values derived from DEMs to field-obtained shielding factors from other sites, showing an agreement of 95 %–99 %.

3.3 Mineral separation

For each sample fragment used, the mean thickness was calculated using a caliper in 5–40 points, and then a sample thickness average was obtained, which was weighted by rock fragment mass. Afterwards, samples were crushed and sieved to obtain a 100–1000 µm size fraction, which was then rinsed to eliminate dust and organic matter and dried at 60 °C.

Density separation was done using a 3.0 g cm^{-3} sodium polytungstate solution, after which the heavy concentrates were leached in a 5 % HF, 2.5 % NaOH bath for 24 h before immersing them in 3 M HCl to remove fluoride precipitates, following Bromley et al. (2014). After checking under a microscope, we leached a second and third time, if necessary, in a 5 % HF, 2.5 % NaOH, and/or 2.5 % HF, 1.25 % NaOH solution, until we achieved total removal of groundmass on most crystals. We then carried out magnetic separation of oxides and magnetic groundmass, and then we finally visually removed the remaining impurities, based on colour and texture, to leave pure pyroxenes (olivines and pyroxenes in the GR samples).

3.4 Geochemical analyses

For each studied lava flow, major and trace element compositions were analysed at the Service d'Analyse des Roches et Minéraux (SARM) of the Centre de Recherches Pétrographiques et Géochimiques (CRPG, Université de Lorraine, Nancy, France) by inductively coupled plasma optical

Figure 2. Examples of targeted sites. Red arrows point to a 20 cm long GPS. Panels **(a)**, **(b)**, **(c)**, and **(d)** represent typical sampled surfaces ('a'ā morphologies). **(a)** A large tumuli standing out 1.5 m above ground level (sample RTp-PD027). **(b)** A large tumuli standing out 2.5 m above ground level (sample DC-PD330). **(c)** Detail of lava top with rough, irregular surfaces resembling 'a'ā lava flow morphologies, which is indicative of minimal erosion (sample MN-PD220). **(d)** 'A'ā block standing out ∼ 40 cm above the ground with a pencil for scale (sample SC-PD001). **(e)** Surface of the Pinnacle Ridge spatter deposit (sample PR-PD085). **(f)** Sampled surface of the Waihohonu Plateau blocky flow (sample WP-PD008).

emission spectroscopy (ICP-OES) and inductively coupled plasma mass spectrometry (ICP-MS), respectively, for both bulk rock and pure pyroxenes and olivines. Each analysed sample consisted of 1 g of powdered rock/minerals that was fused at 980 °C for 60 min in Pt crucibles together with ultrapure $LiBO_2$ in a 1 : 3 ratio prior to glass dissolution and measurements. The complete procedure is described in detail in Carignan et al. (2001).

3.5 Measurement of helium isotope concentrations

We analysed ^{3}He and ^{4}He concentrations in pyroxenes and olivines using a GV Instruments Helix Split Flight Tube multi-collector noble gas mass spectrometer attached to a gas line at CRPG (e.g. Schimmelpfennig et al., 2011; Blard et al., 2013, 2015).

Pure minerals were wrapped in tin capsules, loaded in a carousel, and baked for one night at 100 °C under ultra-high vacuum. The samples were heated to > 1300 °C for

15 min in a full metal induction furnace (Zimmermann et al., 2018), and the expelled gases were purified using four activated charcoal traps at 77 K in order to trap large amounts of CO_2, H_2O, N_2, and heavy noble gases (Ar, Kr, and Xe) from the melted samples by physisorption. In parallel, four getters initially activated at 800 °C were used at room temperature to trap all reactive species (e.g. H_2O, CO_2, N_2, and O_2) by chemisorption. After these two steps, He was condensed using a cryogenic trap at 12 K under ultra-low pressure ($0.5–1 \times 10^{-8}$ mbar) and then released at 75 K towards the mass spectrometer that measured, in static mode, ^{3}He and ^{4}He. The source settings were adjusted to get the best compromise between linearity, sensibility, and stability (e.g. ^{3}He sensitivity $= 4.30 \times 10^{18} \pm 5$ % cps mol^{-1} and ^{4}He sensitivity $= 7.45 \times 10^{13} \pm 2$ % mV mol^{-1}). HESJ gas standards (20.63 R/Ra, Matsuda et al., 2002, Ra: atmospheric ^{3}He/^{4}He ratio of 1.39, Lupton and Evans, 2013) were measured daily with a reproducibility of 4.7 %, and ^{4}He and ^{3}He values were also routinely compared with CRONUS-P standards (Blard et al., 2015; Schaefer et al., 2016, reproducibility of 5.0 %). The main source of background He (measured daily with typical ^{3}He blanks $< 5 \pm 3.5 \times 10^3$ atoms, typical ^{4}He blanks of $1.3 \times 10^9 \pm 1.8 \times 10^8$ atoms, and ^{3}He/^{4}He ratios similar to 1 Ra) was the Ta crucible, which was degassed at 1800 °C for 30 min prior to the analyses.

Crushed–released He isotopic analyses (used for magmatic corrections) were performed in samples with larger crystals (dominant fraction of 500–1000 µm, which were shown to contain larger amounts of magmatic He likely hosted in melt inclusions; Puchol et al., 2017) using a soft iron slug activated by external solenoids. Samples were crushed for 5 to 7 min at 100 strokes per minute with tube-specific ^{3}He blanks between 3.8 ± 1.1 and $0.6 \pm 0.3 \times 10^4$ atoms and ^{4}He blanks between $3.1 \pm 0.1 \times 10^9$ and $2.0 \pm 1.8 \times 10^8$ atoms. For a detailed description of the in vacuo crushing He extraction method, see Puchol et al. (2017).

3.6 Surface exposure age determinations

3.6.1 Calculation of cosmogenic ^{3}He

To correctly determine the concentration of $^3\mathrm{He}_{\mathrm{cos}}$, it is necessary to consider the non-cosmogenic contributions to total ^{3}He measured when fused in vacuo ($^3\mathrm{He}_{\mathrm{tot}}$), which is described as

$$^3\mathrm{He}_{\mathrm{tot}} = {}^3\mathrm{He}_{\mathrm{cos}} + {}^3\mathrm{He}_{\mathrm{atm}} + {}^3\mathrm{He}_{\mathrm{nuc}} + {}^3\mathrm{He}_{\mathrm{mag}}, \quad (1)$$

where $^3\mathrm{He}_{\mathrm{atm}}$ is the atmospheric ^{3}He hosted at the minerals' surfaces as a contaminant and is time-independent. $^3\mathrm{He}_{\mathrm{nuc}}$ is the nucleogenic ^{3}He produced by capture of low-energy neutrons emitted by ^{6}Li and dependent on Li concentrations in the mineral, U and Th concentrations in the rock, and the mineral closure age (equivalent to eruption age for pyroxenes and olivines in volcanic rocks, Kurz, 1986a). $^3\mathrm{He}_{\mathrm{mag}}$ is the magmatic ^{3}He contribution (time-independent) present in melt and fluid inclusions and within the matrix of the minerals.

Atmospheric He (both ^{3}He and ^{4}He) concentrations are inversely proportional to the mineral grain size and become insignificant for minerals larger than 100 µm (Blard, 2021), so they were considered non-existent in our calculations. $^3\mathrm{He}_{\mathrm{nuc}}$ quotas are normally negligible for uneroded lava flows in which the closure and exposure ages are the same (Kurz, 1986a), as shown by our calculations (Table A3) based on the spreadsheet developed by Blard (2021).

The total contribution of $^3\mathrm{He}_{\mathrm{mag}}$ was accounted for in Eq. (3) and estimated using a magmatic ratio obtained as an uncertainty-weighted average from isotopic analyses of three samples crushed in vacuo and previous data from pyroxene and olivine phenocrysts in the Waimarino and Ohakune basalts (Sect. 4.2 and Supplement files S2.1 and S2.2).

The total amount of ^{4}He measured in each sample ($^4\mathrm{He}_{\mathrm{tot}}$) is defined by the following equation:

$$^4\mathrm{He}_{\mathrm{tot}} = {}^4\mathrm{He}_{\mathrm{mag}} + {}^4\mathrm{He}_{\mathrm{atm}} + {}^4\mathrm{He}_{\mathrm{rad}} + {}^4\mathrm{He}_{\mathrm{cos}}, \quad (2)$$

where $^4\mathrm{He}_{\mathrm{mag}}$ corresponds to the time-independent magmatic ^{4}He quota naturally present in the minerals, while $^4\mathrm{He}_{\mathrm{atm}}$ accounts for atmospheric ^{4}He contaminating the minerals' surfaces (time-independent). $^4\mathrm{He}_{\mathrm{rad}}$ is generated by the decay of radioactive isotopes present in the minerals (such as U, Th, and Sm) and dependent on the abundance of these elements in the minerals and the closure age. Crystals normally exhibit an enriched ^{4}He exterior rim generated by implanted $^4\mathrm{He}_{\mathrm{rad}}$ from the matrix (Lal, 1989), typically with higher concentrations of U, Th, and Sm. $^4\mathrm{He}_{\mathrm{cos}}$ refers to the cosmogenic contribution of ^{4}He, which is negligible compared to other non-cosmogenic varieties of ^{4}He (Blard, 2021) and is therefore also omitted from our calculations.

In this paper, we follow the approach of Blard and Farley (2008), which corrects for the contributions of $^4\mathrm{He}_{\mathrm{rad}}$, $^4\mathrm{He}_{\mathrm{mag}}$, and $^3\mathrm{He}_{\mathrm{mag}}$ for uneroded lava flows using the following equation:

$$^3\mathrm{He}_{\mathrm{cos}} = \frac{^3\mathrm{He}_{\mathrm{tot}} - {}^4\mathrm{He}_{\mathrm{tot}}\left(\frac{^3\mathrm{He}}{^4\mathrm{He}}\right)_{\mathrm{mag}}}{R}, \quad (3)$$

where R (or R factor) is defined by

$$R = 1 - \left(\frac{P_4}{P_3}\right)\left(\frac{^3\mathrm{He}}{^4\mathrm{He}}\right)_{\mathrm{mag}}, \quad (4)$$

where P_4 and P_3 are the $^4\mathrm{He}_{\mathrm{rad}}$ and local $^3\mathrm{He}_{\mathrm{cos}}$ production rates.

The use of the R factor is essential when using $^3\mathrm{He}_{\mathrm{cos}}$ to date uneroded lava flows as it permits the incorporation of a time-dependent $^4\mathrm{He}_{\mathrm{rad}}$ quota, avoiding the issue of an underestimation or overestimation of the $^4\mathrm{He}_{\mathrm{mag}}$ (and, hence, $^3\mathrm{He}_{\mathrm{mag}}$) contribution.

Individual values of P_4 were calculated for each lava flow using the spreadsheet developed by Blard (2021), neglecting the implanted $^4He_{rad}$ component to account for the removal of the ^{4}He-enriched crystal rim with HF leaching.

Sample-specific P_3 estimates were obtained following the Lal–Stone time-corrected scaling scheme (Lal, 1991; Stone, 2000; Nishiizumi, 1989; Balco et al., 2008) using the online calculator "Cosmic Ray Exposure program" (CREp; https://crep.otelo.univ-lorraine.fr/, last access: 25 May 2024; Martin et al., 2017) and the global $^3He_{cos}$ production rate database therein.

3.6.2 Determination of exposure and eruption ages

To obtain exposure ages, we used the CREp online calculator, which calculated exposure ages based on our $^3He_{cos}$ concentrations and scaling parameters, the Lal–Stone time-corrected scaling scheme (Lal, 1991; Stone, 2000; Nishiizumi, 1989; Balco et al., 2008), the ERA-40 atmosphere model (Uppala et al., 2005), the geomagnetic framework of Muscheler et al. (2005), and the worldwide mean $^3He_{cos}$ production rates of 122 ± 12 at g^{-1} yr^{-1} at sea level and high latitudes (SLHL).

Exposure ages calculated using the LSD scaling scheme (Lifton et al., 2014) and different atmospheric models and geomagnetic databases are available in the Supplement (file S3), showing variations of 1 %–3 % compared with the exposure ages calculated using the parameters outlined above. This is, however, not the case of the LSD geomagnetic framework, which provides exposure ages between 8.6 % and 3.8 % younger. This discrepancy can be explained by a higher spatial variability in the LSD framework than other models and especially by the model's relative scaling factor high over the Aotearoa / New Zealand region during the Holocene (Lifton, 2016). New paleosecular variation records based on Aotearoa / New Zealand lake sediment cores (Turner et al., 2015; Turner and Corkill, 2023) suggest that this scaling factor high is a spatial artefact caused by the small number of Southern Hemisphere records used to make up the global model of the LSD framework. Thus, we place greater emphasis on results produced using models that do not contain such effects (e.g. Muscheler et al., 2005; Lifton, 2016).

$^3He_{cos}$ production rates have been shown to be indistinguishable in clinopyroxenes and orthopyroxenes (Delunel et al., 2016), justifying our decision to use a worldwide mean production rate estimate for our exposure age determinations. Additionally, this production rate value is supported by a local calibration test using the radiocarbon-dated debris avalanche deposits of the Murimotu Formation on the outer northwestern slopes of Ruapehu (Eaves et al., 2015). Despite some studies that suggested that olivines concentrate slightly larger amounts of $^3He_{cos}$ compared to pyroxenes (Ackert et al., 2003; Fenton et al., 2009), the difference was almost statistically insignificant, and, in a more recent study, Fenton and Niedermann (2014; as well as previous data from Blard et al., 2006) provided results implying that olivine and pyroxenes have similar amounts of $^3He_{cos}$.

We measured three to five samples per lava flow to counter the possibility that individual samples may be affected by erosion or shielding that would compromise their accuracy for constraining the time of lava flow emplacement. To derive single exposure ages for lava flows from these multiple measurements, we used each sample's internal age uncertainty (1σ, not including the external uncertainty from P_3) and implemented the summary age statistics and outlier removal routine contained in version 3 of the Balco et al. (2008) online exposure age calculator, described in the documentation (Sect. 4.C, available at https://sites.google.com/a/bgc.org/v3docs/, last access: 25 May 2024). In summary, we used weighted mean summary ages if the samples formed a single population at the 95 % confidence interval using the chi-squared statistic (outliers are indicated in italics throughout Sect. 4.4). If this result could not be achieved by incremental outlier removal while maintaining a sample population ≥ 3, then we used the mean and standard error as the summary age of the lava flow. We finally propagated the P_3 uncertainty into all summary ages (reported with their 2σ interval), which is necessary when comparing TCN-based eruption ages to those from other geochronological methods (e.g. $^{40}Ar/^{39}Ar$). In the case of flows for which fewer than three samples passed the single population test (or only two samples were analysed), we considered the summary age to be a minimum eruption age. For those flows with three or more exposure ages passing this test, summary ages were considered robust eruption ages. We used internal 2σ intervals (INT 2σ, not including P_3 errors) to compare intra-site and inter-site age distributions and clustering.

4 Results

4.1 Bulk rock and mineral geochemistry

Major and trace element concentrations of bulk rocks and minerals from each of the lava flows studied can be found in Table A2.

All bulk rock analyses yielded basaltic andesite to andesitic compositions according to the classification scheme of Le Maitre (2002). Our results indicate that, from the sampled flows, younger flows tend to be less evolved than older flows (Fig. 3a).

Most flows have a bulk geochemistry similar to the reported ranges (Conway et al., 2016) for the respective units they were classified as (Townsend et al., 2017). The only exception is the site here referred to as NR, which shows higher MgO (6.22 wt %) and lower Na_2O (2.95 wt %) than other samples of the Makotuku Member (2 wt %–3 wt % and 3.4 wt %–4 wt %, respectively; Conway et al., 2016). Instead, major element geochemistry of our NR sample matches that of the Mangaehuehu Member (4.7 wt %–7 wt % MgO and

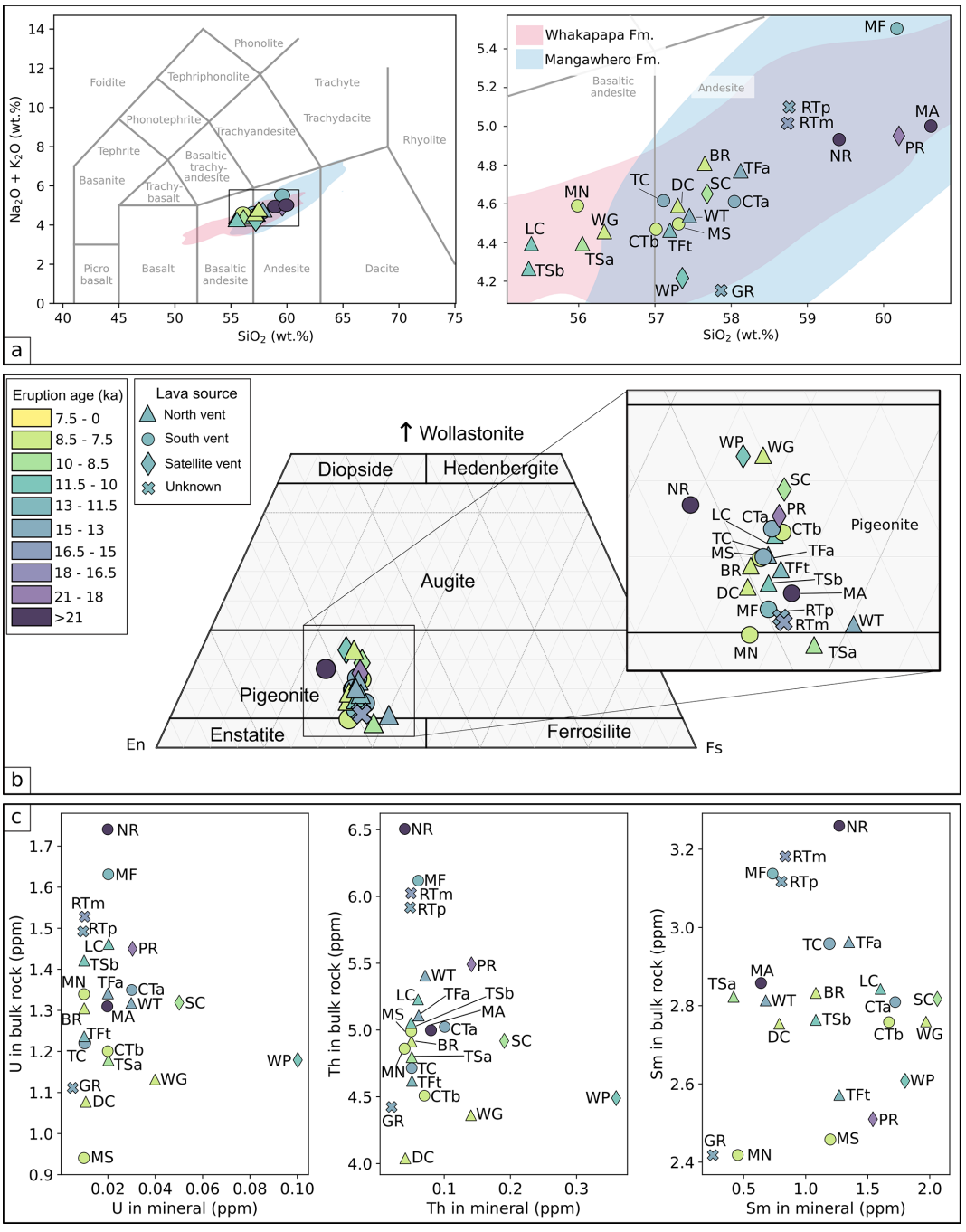

Figure 3. **(a)** TAS classification diagram of the sampled lava flows (Le Maitre, 2002). Coloured areas represent geochemical ranges of Whakapapa and Mangawhero lavas. **(b)** Pyroxene compositions according to the classification scheme of Morimoto et al. (1988). Each triangle represents the average geochemistry of each lava flow's pyroxene population. **(c)** U, Th, and Sm concentrations in the samples. The *x* and *y* axes represent the maximum concentrations in minerals (pyroxenes and olivines) and in bulk rock, respectively.

3 wt %–3.4 wt % Na_2O; Conway et al., 2016), the lavas of which are significantly older (Table 1).

Mineral geochemistry shows that, on average, the pyroxenes are pigeonite (Fig. 3b), although analyses of modal phases of Ruapehu lavas (Hackett, 1985; Conway, 2016) suggest that this represents a combination of augite and enstatite crystals. MN and TSa yield average compositions of enstatite phases, indicating that the orthopyroxene phase dominates over the clinopyroxene in these flows. The analysed olivines (sample GR-PD023) are magnesium-rich (Fo_{69}; Table A2). Comparing the obtained average compositions with previous $^3He_{cos}$ studies, our pyroxenes show higher contents of or-

thopyroxene than those analysed by Blard et al. (2006) and higher clinopyroxene contents than samples of Eaves et al. (2015).

In general, trace element concentrations are relatively homogeneous across the sampled sites. Figure 3c shows the concentrations of the main radioactive elements producing $^4He_{rad}$ (U, Th, and Sm) in bulk rock and in the mineral phases (pyroxenes and olivines). Bulk rocks contain 0.94–1.74 ppm U, 4.04–6.50 ppm Th, and 2.41–3.25 ppm Sm, while pyroxenes contain 0.01–0.10 ppm U, 0.04–0.36 ppm Th, and 0.44–2.07 ppm Sm (uncertainties $< 20\,\%$ and detection limits of 0.01 ppm). Note that U and Th concentrations in the rock are not involved in the production of the measured $^4He_{rad}$, as the external crystal rims were removed before the analyses. GR olivines have lower contents of these elements (with U below the detection limit) and, therefore, larger P_4 associated errors. However, element concentrations provided for minerals represent maximum values, as there is a possibility of groundmass and/or melt inclusion contamination that may not be accounted for at the time of measurement. These values indicate (maximum) partition coefficients (Kd) of 0.006–0.085 for U, 0.006–0.080 for Th, and 0.15–0.74 for Sm in pyroxenes and 0.045 for U, 0.045 for Th, and 0.11 for Sm in olivines. The pyroxene maximum Kd values, in general, agree with values from the literature (Dostal et al., 1983; Luhr and Carmichael, 1980; Gallahan and Nielsen, 1992; Nicholls and Harris, 1980). Those values for U and Th in olivines are similar to those reported by Dunn and Sen (1994) and Villemant (1988), while the Kd for Sm in our olivines is an order of magnitude larger than that of Dunn and Sen (1994), which can be explained by the impact of fluid inclusions with higher Sm contents within the olivine crystals.

4.2 Local magmatic ^{3}He/^{4}He ratio

We measured ^{3}He and ^{4}He released after in vacuo crushing for samples MA-PD058, WG-PD326, and DC-PD329 (data available in Supplement file S2.1). These values result in ^{3}He/^{4}He ratios of 5.5 ± 1.0, 17.9 ± 6.9, and $9.2 \pm 6.1 \times 10^{-6}$ for each sample, respectively. The large uncertainties associated with the ratios measured in samples WG-PD326 and DC-PD329 are a result of the low total ^{4}He values ($<5 \times 10^9$ at g^{-1}).

We used the three measured ^{3}He/^{4}He values and two ratios from Patterson et al. (1994) to constrain the local magmatic ^{3}He/^{4}He value. These are $6.5 \pm 2.4 \times 10^{-6}$ (Ohakune basalt pyroxenes, one sample) and $8.6 \pm 3.7 \times 10^{-6}$ (Waimarino basalt olivines, mean of three aliquots from one sample), which are comparable to those obtained by in vacuo crushing of our samples. All analyses from Patterson et al. (1994) are from fused samples (and not from in vacuo crushed samples, which is the standard approach to release predominantly magmatic He; Kurz, 1986b), but we assumed that all the measured ^{3}He and ^{4}He have a magmatic origin, as the samples come from flow interiors of young flows (i.e. they likely contain low $^4He_{rad}$ and minimal to no $^3He_{cos}$). With these data, we calculated an uncertainty-weighted mean ^{3}He/^{4}He ratio using IsoplotR (Vermeesch, 2018) and obtained a value of $5.9 \pm 2.6 \times 10^{-6}$ (or 4.2 ± 1.9 Ra; see Supplement file S2.2), which we used for the magmatic corrections in this study. The impact of the obtained magmatic ratio and its uncertainty in our results is described in Sect. 4.3.

4.3 Fusion-released helium isotopes and cosmogenic ^{3}He concentrations

We analysed a total of 77 samples from 23 individual flows. All fusion ^{3}He and ^{4}He measurements, calculated $^3He_{cos}$ concentrations, and derived exposure and eruption ages are shown in Table 2. Measured ^{3}He varies between 2.1×10^6 and 2.4×10^7 at g^{-1}, with 2 %–7 % of relative associated error (1σ). $^4He_{tot}$ values are surprisingly low across most of our samples (possibly due to the repeated HF-leaching steps the samples were exposed to prior to analysis; see Bromley et al., 2014), typically ranging between 0.3 and 9.6×10^{10} at g^{-1} with uncertainties between 0.04 and 0.18×10^{10} at g^{-1}. These values normally result in total ^{3}He/^{4}He ratios of 130–800 Ra, although they are lower (50–90 Ra) or higher (1200–1500 Ra) in some cases (see Table 2).

The complete detail of all sources of corrections is available in Table A3 and in Supplement file S4. Calculated $^3He_{nuc}$ production rates (P_{nuc}) are 4 orders of magnitude below P_3 values, making $^3He_{cos}$ results insensitive to nucleogenic corrections. P_4 ranges between 4×10^4 and 3×10^5 at g^{-1} yr^{-1}. We assume a 10 % error associated with all P_4 results except for the site GR, which has lower concentrations of radioactive elements (and, hence, the lowest P_4 number within our lavas) with uncertainties of 20 %–40 %, for which we considered a 25 % uncertainty in our P_4 estimates. Uncertainties associated with the calculated local magmatic ^{3}He/^{4}He ratio represent $< 10\,\%$ of the informed error associated with $^3He_{cos}$ results. This ratio, combined with our P_4 calculations (3.5×10^4–6.1×10^5 at g^{-1} yr^{-1}) and local P_3 values between 313 and 584 at g^{-1} yr^{-1} (elevations between 1288 and 2148 m a.s.l.), yields R factors > 0.99 (Table A3). This indicates that, even if the measured concentrations of radioactive elements in our minerals represent maximum values, corrections for $^4He_{rad}$ have a minor ($< 1\,\%$) impact on our final $^3He_{cos}$ values. The $^3He_{cos}/^3He_{tot}$ ratios calculated for our samples vary between 0.90 and 0.99, implying that the $^3He_{cos}$ quota dominates over magmatic (and nucleogenic) ^{3}He.

The used magmatic ^{3}He/^{4}He ratio ($5.9 \pm 2.6 \times 10^{-6}$ or 4.2 ± 1.9 Ra) is derived from only three samples from Ruapehu crushed in vacuo (this study) and two samples from the Ohakune and Waimarino basalts (data from fused samples; Patterson et al., 1994), and it is therefore not well constrained. However, this does not significantly affect our final

results due to the low $^4He_{tot}$ measured in most of our samples. To demonstrate this, we estimated the resulting $^3He_{cos}$ concentration if the magmatic $^3He/^4He$ ratio of the sample SC-PD001 (which has the smallest measured $^3He/^4He$ ratio across our samples and is, hence, the most sensitive to this test) was 8.4 and 2.1 Ra (twice and half the mean value of 4.2 Ra used for our calculations and covering most of the range globally observed in subduction zone volcanism; Hilton et al., 2002). This test yields $^3He_{cos}$ concentrations of 3.28 ± 0.31 and $3.71 \pm 0.31 \times 10^6$ at g^{-1} (resulting in exposure ages of 9.74 ± 0.85 and 10.91 ± 0.83 ka) with magmatic ratios of 8.4 and 2.1 Ra, respectively, both falling within the error of the concentration obtained using a magmatic ratio of 4.2 ± 1.9 Ra for SC-PD001 ($3.57 \pm 0.31 \times 10^6$ at g^{-1} and an exposure age of 10.53 ± 0.83 ka). This indicates that the potentially variable magmatic $^3He/^4He$ ratios present in our samples do not significantly impact our results, although they might partially explain small differences between the obtained exposure ages of samples from the same flow.

4.4 Lava flows: background and new cosmogenic ^{3}He constraints

We obtained 16 eruption ages and 7 minimum eruption ages (Table 2) based on the criteria defined in Sect. 3.6.2.

4.4.1 Iwikau Member (Whakapapa Formation)

The Iwikau Member of the Whakapapa Formation covers a large area on the northwestern and eastern flanks of Ruapehu (Fig. 1) and is subdivided into three flow packages: Tawhainui, Mangatoetoenui, and Taranaki Falls flows (Fig. 4a, b), all interpreted to have originated from Ruapehu's northern vent (Townsend et al., 2017).

Tawhainui flows

The Tawhainui flows comprise a voluminous sequence of lava flows on the northwestern slopes of the volcano. They have been the most studied unit of Ruapehu due to their accessibility and availability of the fresh exposures of flow interiors, facilitated by the construction of the largest ski field in Te Ika-a-Māui / North Island. We sampled three flows from this unit: the Delta Corner flow (DC samples), the Bruce Road flow (BR samples, both after Greve et al., 2016), and the Whakapapa Glacier flow (WG samples).

The fresh-looking Delta Corner flow was previously dated at 6.0 ± 2.4 ka with $^{40}Ar/^{39}Ar$ by Conway et al. (2016), and this age was refined to 8200–7900 BP by Greve et al. (2016) based on paleomagnetic data. Analyses from three samples from an area with distinct 'a'ā surface morphologies (see Fig. 2b) yield well-clustered exposure ages, which result in an eruption age of 7.8 ± 1.5 ka. Our results are consistent with the age range of 8200–7900 BP provided by Greve et al. (2016), suggesting that the flow's true age lies on the upper end of the uncertainty provided by Conway et al. (2016).

The Bruce Road flow is a large 'a'ā flow that underlies the Delta Corner flow and has been constrained to 8800–8500 BP by Greve et al. (2016) using paleomagnetism. Downslope from the BR sample site, the flow has unclear boundaries, as it is covered by vegetation. Based on four individual exposure ages (7.4, 8.1, 7.8, and 9.1 ka), we obtained an eruption age of 8.1 ± 2.1 ka for the Bruce Road flow, which is consistent with its paleomagnetic constraint.

The Whakapapa Glacier flow is one of the youngest lavas of the sequence based on stratigraphic relations, which suggest a comparable age to that of the Delta Corner flow. Due to the highly eroded nature of the Whakapapa Glacier flow's surface, only two WG samples were collected, which yield a minimum eruption age of 7.8 ± 2.4 ka. This result is consistent with the stratigraphy and the age of the Delta Corner flow.

Mangatoetoenui flows

This subunit includes a group of lava flows on the eastern slopes of Ruapehu, and its age is poorly constrained (Table 1). We sampled four individual flows classified based on geochemistry and location within the Mangatoetoenui flows: Lava Cascade (LC samples), Tukino Slopes-a (TSa samples), Tukino Slopes-b (TSb samples), and Tukino Flats (TFt samples) flows (Fig. 4b).

The LC sample site is interpreted to be part of an approximately 4 km long lava flow terminating at a 20 m high lava cascade at 1620 m a.s.l. This flow was described in detail by Rhodes (2012) and dated on a cliff at its terminus at 0.8 ± 5.6 ka by Conway et al. (2016). We analysed four individual samples from an outcrop located ~ 1 km upslope from the lava toe and obtained an eruption age of 11.4 ± 2.3 ka for the Lava Cascade flow (outside the 2σ interval of Conway et al., 2016; see Sect. 5.1), with one young outlier removed (sample LC-PD256). The outlier can be explained by local erosion, shielding from a now collapsed neighbouring lava tumuli (and hence an underestimation of the shielding factor) or a period of tephra cover that could have reduced the ^{3}He production on the surface sampled.

The Tukino Slopes-a flow has not been previously dated, but its location and stratigraphic position suggest a similar eruption age to the Lava Cascade and Tukino Slopes-b flows. All measured TSa samples (8.7, 9.5, and 9.9 ka) form a single population and provide an eruption age of 9.4 ± 1.8 ka, in good agreement with the stratigraphy.

The TSb sample site likely corresponds to the same flow dated with $^{40}Ar/^{39}Ar$ at 9.2 ± 8.0 ka by Conway et al. (2016). We obtained exposure ages of 10.5, 11.9, and 11.9 ka for the TSb samples, which result in a refined eruption age of 11.5 ± 2.2 ka for the Tukino Slopes-b flow. The eruption age we obtained for the Tukino Slopes-b flow is consistent with (and more precise than) the existing radiometric age and, as

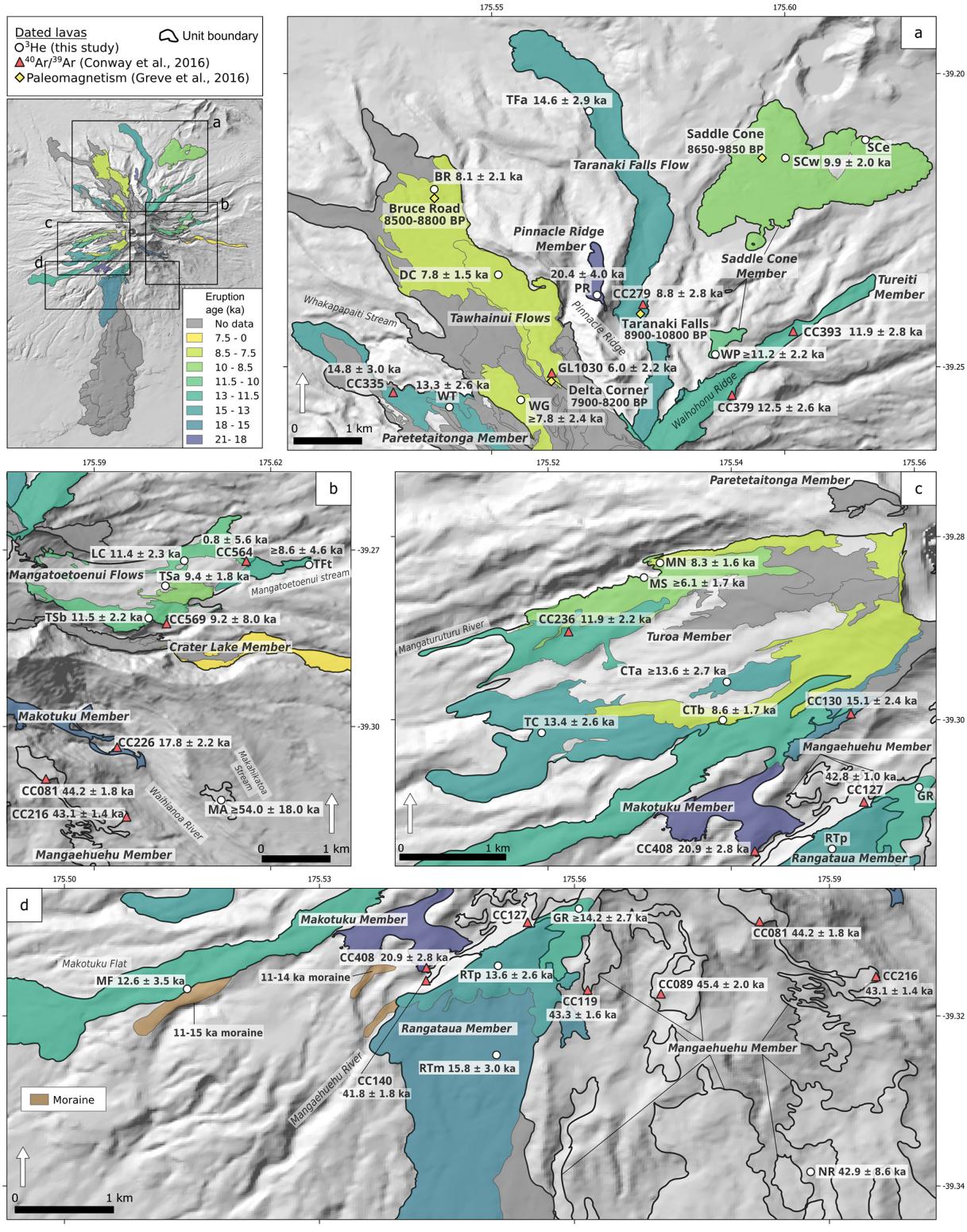

Figure 4. Map of dated < 21 ka lava flows on **(a)** northern, **(b)** eastern, **(c)** western, and **(d)** southern Ruapehu. Polygons redefined from Townsend et al. (2017). Boundaries of the Mangaehuehu Member (Mangawhero Formation), as of Townsend et al. (2017), shown for context of site NR of this study. The shaded-grey areas represent postglacial flows without chronological data.

suggested by the stratigraphy, similar to the age of the Tukino Slopes-a flow.

The TFt sample site is located at a lower elevation ($\sim$ 1515 m a.s.l.), and its stratigraphic position suggests a similar or older age than the rest of the Mangatoetoenui flows. Our results for three TFt samples (7.7, 10.8, and 7.3 ka) do not form a single population and result in a minimum eruption age of 8.6 ± 4.6 ka for the Tukino Flats flow. The older exposure age (10.8 ka) is difficult to explain as an outlier, as the presence of inherited ^{3}He is not justifiable for lava flows, whereas the younger ages may be explained as outliers owing to surface erosion or temporal burial by alluvium or tephra. Lack of additional samples hindered our ability to obtain a robust eruption age. Considering a minimum eruption age of 8.6 ± 4.6 ka, the ages of the other flows from the Mangatoetoenui flows, and their stratigraphic position, our best estimate for the Tukino Flats flow is 12–10 ka.

Taranaki Falls flow

The Taranaki Falls flow (TFa samples) is a rootless (not continuous towards the vent it would have been erupted from), elongated lava flow that outcrops discontinuously for $\sim$ 8 km almost directly to the north of the volcano's summit area (Townsend et al., 2017, Fig. 4a) and terminates at the 20 m waterfall after which it is named. The flow was dated with ^{40}Ar/^{39}Ar at 8.8 ± 2.8 ka by Conway et al. (2016). Based on this date, Greve et al. (2016) found two age ranges (10 800–10 200 and 9500–8900 BP) with a better match to the local paleosecular variation record.

We sampled the flow at an outcrop 800 m upstream from the flow terminus and obtained exposure ages of 14.6, 14.2, and 15.0 ka, resulting in an eruption age of 14.6 ± 2.9 ka, which is outside the confidence interval of the radiometric age (see Sect. 5.1).

4.4.2 Saddle Cone Member (Whakapapa Formation)

This unit comprises a large, lobate 'a'ā flow originating from a parasitic cone on the north-northeastern side of Ruapehu that is almost disconnected from the main edifice (Fig. 4a). The only available constraint for this flow was provided by Greve et al. (2016), who suggested an age of 9850–8650 BP based on paleomagnetic analyses of samples from the western lobe of the flow. The Saddle Cone Member also includes a smaller blocky lava flow lying between this cone and Ruapehu's summit region (that likely originated from a satellite vent), adjacent to the Waihohonu Ridge and here referred to as the Waihohonu Plateau flow, which was linked to the main Saddle Cone deposits by its geochemical similarity and location. Nairn et al. (1998) suggested that the Waihohonu Plateau ("1990 m lava" therein) might be younger than 5 ka as no deposits from the Papakai tephra were found above the flow.

Individual exposure ages of samples from the main western lobe of the Saddle Cone lavas (SCw samples; 10.5, 10.2, and 9.2 ka, Fig. 2b) show good agreement. Additionally, we analysed a sample from the eastern lobe (SCe, whose surface elevation is more than 100 m below that of the main lobe; see Fig. 4a) to test the hypothesis of a multi-episodic origin. The obtained exposure age of this sample is 9.6 ka (Table 2), indistinguishable from those of the western lobe. We suggest a single eruption age of 9.9 ± 2.0 ka ($n = 4$) for both lobes, which is consistent with the existing paleomagnetic constraint for this flow.

The blocky nature of the Waihohonu Plateau flow made it difficult to find uneroded surfaces, and only two samples were obtained (WP samples, Fig. 2f). Analyses from these samples result in a minimum eruption age of 11.2 ± 2.2 ka.

4.4.3 Pinnacle Ridge Member (Whakapapa Formation)

The Pinnacle Ridge Member is a welded spatter deposit (Fig. 2e) linked to a dike on a ridge of the same name on the northern flanks of the volcano (Fig. 4a). Due to its geochemistry and geographic location, Donoghue et al. (1999) linked this isolated spatter-fed lava deposit to the Taurewa pyroclastic unit (ca. 10 ka) described by Topping and Kohn (1973), manifested as a tephra layer with isopachs centred on the northern flanks of Ruapehu.

PR samples yield exposure ages of 20.8, 19.0, and 21.5 ka, resulting in an eruption age of 20.4 ± 4.0 ka for this unit, which is at least 10 kyr prior to the Taurewa eruptive event.

4.4.4 Rangataua Member (Whakapapa Formation)

The Rangataua Member includes the longest and most voluminous known lava flow of Ruapehu ($\geq$ 15 km long and ~ 1.5 km^3). It first outcrops $\sim$ 3.5 km south from the summit, which led to the hypothesis that it is sourced from a satellite vent (Hackett, 1985; Price et al., 2012), although Townsend et al. (2017) suggest initial transport over ice as a possible alternative explanation for its rootless nature. Based on geochemical differences, this unit was first subdivided by Price et al. (2012) into proximal, medial, and distal flows (the latter being the largest flow of the sequence). They suggested eruption ages of 12–10 ka based on underlying and overlying tephra sequences (unpublished data). These lavas overlie left lateral moraines at 1600–1400 m a.s.l., which have been correlated to right lateral moraines of the Mangaehuehu River valley dated at 11–14 ka (Eaves et al., 2019) using ^{3}He$_{cos}$ dating (Fig. 4d). We sampled the Rangataua Member at two locations: one close to the highest outcrops (RTp, "proximal") and another one approximately 1 km to the south (RTm, "medial"). We did not sample the distal flows, which are interpreted to be older than the medial flows, due to vegetation cover (Fig. 1c).

RTp samples (e.g. Fig. 2a) yield exposure ages of 13.9, 12.4, 13.9, and 14.4 ka and a final eruption age of

13.6 ± 2.6 ka. Results of RTm samples (16.2, 16.0, 15.3, and *8.2* ka) include a young outlier, but the remaining samples are internally consistent and indicate an eruption age of 15.8 ± 3.0 ka, which agrees with the field relationships of the area, as this flow underlies RTp, but not so with previous age estimates (see Sect. 5.1). The ages of the Rangataua proximal and medial flows and their INT 2σ uncertainties (13.6 ± 0.6 and 15.8 ± 0.8, respectively) do not overlap, indicating that they correspond to different eruptive episodes.

4.4.5 Paretetaitonga Member (Whakapapa Formation)

The Paretetaitonga Member comprises a series of lava flows that likely originated from the northern summit vent of Ruapehu and emplaced in the headwaters of the Whakapapaiti Stream, northwest of the summit area (Fig. 4a). We sampled one lava flow (Whakapapaiti flow, WT samples) stratigraphically higher than the only flow dated from this unit (14.8 ± 3.0 ka; Conway et al., 2016).

We obtained exposure ages in good agreement with each other (12.8, 13.4, and 13.7 ka), resulting in an eruption age of 13.3 ± 2.6 ka, consistent with the existing chronology.

4.4.6 Turoa Member (Whakapapa Formation)

The Turoa Member corresponds to a sequence of numerous flows extending directly west from the edge of Ruapehu's crater rim and reaching the Mangaturuturu valley bottom. Based on the distributions of the flows and two ^{40}Ar/^{39}Ar dates (Table 1), this unit is assumed to have been formed by effusive activity from the southern summit vent at ca. 17–10 ka. We sampled five sites, distributed on the northern (MN and MS), central (CTa and CTb), and western (TC) areas (Fig. 4c), covered by this unit.

The Mangaturuturu North flow corresponds to a flow on the headwaters of the Mangaturuturu Stream, and, due to stratigraphic relations and flow morphologies, it was suspected to be the youngest lava on western Ruapehu. We analysed five surfaces of the Mangaturuturu North flow (MN samples, Fig. 2c, with exposure ages of 8.0, 8.9, *6.0*, 8.9, and 7.7 ka), and, eliminating the young outlier of 6.0 ka, they yield a robust eruption age of 8.3 ± 1.6 ka.

The Mangaturuturu South flow underlies the Mangaturuturu North flow and extends down ~ 3 km from the summit area. Poor exposures of original flow surfaces prevented us from collecting more than three samples from the Mangaturuturu South flow (MS samples). Additionally, purification of the minerals in these samples was incomplete due to high (> 50 %) mass loss with each HF-leaching cycle, and we suspect an overestimation of measured pyroxene mass for these samples. Sample analyses result in exposure ages that do not pass the single population test (Table 2) but provide a minimum eruption age of 6.1 ± 1.7 ka.

The Central Turoa-a and Central Turoa-b flows are located close to each other and at a similar elevation south of the MN and MS sample sites. We only collected two samples from the Central Turoa-a flow (CTa) due to a lack of suitable surfaces, which suggest a minimum eruption age of 13.6 ± 2.7 ka. Three out of the four analysed Central Turoa-b flow samples (CTb samples, which yielded exposure ages of *4.9*, 8.8, 8.4, and 8.5 ka) show good agreement and yield an eruption age of 8.6 ± 1.7 ka. These results indicate that the Central Turoa-a and Central Turoa-b flows correspond to two different eruptive episodes.

The Turoa Cascades flow (TC samples) is a large flow that reaches the Mangaturuturu River valley floor, and its stratigraphic position indicates that it is likely the oldest flow of the Turoa Member. Individual exposure ages of the TC samples (*11.4*, 14.1, 13.1, and 13.3 ka) include a young outlier and indicate an eruption age of 13.4 ± 2.6 ka for the Turoa Cascades flow, which is in good agreement with the rest of the ages obtained for the Turoa Member lavas.

4.4.7 Makotuku Member (Mangawhero Formation)

We sampled three flows previously mapped as part of the Makotuku Member of the Mangawhero Formation: the Makotuku Flat flow (MF samples) on the southwest and the Ngā Rimutāmaka and Makahikatoa flows (NR and MA samples, named after local site and stream, respectively) on the south of Ruapehu's edifice. The spatial distribution of Makotuku lavas suggests that they originated from the southern summit vent.

The Makotuku Flats flow extends to the west of the edifice, reaching the Makotuku valley bottom (Fig. 4d), and overlies a 11–15 ka moraine (Townsend et al., 2017) at the sampled site. Although results of analyses of MF samples are not particularly well clustered, they behave as a single population and provide an eruption age of 12.6 ± 3.5 ka.

Analyses of NR samples yield well-clustered exposure ages, and we interpret an eruption age of 42.9 ± 8.6 ka, which corresponds to the only date provided for this lava flow so far. It is worth noting that this age and the geochemical composition of this flow match with the ^{40}Ar/^{39}Ar ages and the high-MgO and low-Al_2O_3 nature of the Mangaehuehu Member lavas (Table 1).

The small area where the Makahikatoa flow outcrops prevented us from obtaining more than two suitable samples, which result in a minimum eruption age of 54.0 ± 18.0 ka, this being the first age constraint for this flow.

These three eruption ages do not contradict previous chronology or stratigraphy, but they do not match the age ranges indicated by the geochemical affinities for the Makotuku Member lavas as described by Conway et al. (2016) and Townsend et al. (2017; see Sect. 5.2).

4.4.8 Mangaehuehu Member (Mangawhero Formation)

We sampled a lava flow (Girdlestone Ridge, GR samples) outcropping on a ridge top ~ 1.5 km south from Ruapehu's

summit and 800 m southwest from Girdlestone Peak. This site was previously mapped as Mangaehuehu Member lavas (Townsend et al., 2017) based on interpretation of aerial imagery. However, the uneroded aspect of the flow's surface observed in the field during this study suggests that it could be younger than previously interpreted. The mineral separation process applied to all samples produced the only olivine concentrate (with a minor pyroxene population) of this study.

Analyses of these samples indicate a minimum eruption age of 14.2 ± 2.7 ka (mean calculated from the two oldest exposure ages after the elimination of two outliers), which represents the first age constraint for this lava flow.

5 Discussion

5.1 Comparison of new cosmogenic ^{3}He ages with previous age constraints

The new Holocene ^{3}He exposure ages yield eruption ages with higher precision than ^{40}Ar/^{39}Ar dates of Conway et al. (2016) for this time range (Fig. 5). Additionally, young (< 20 ka) ^{40}Ar/^{39}Ar ages of individual samples have normally weak isochrons, as the R values for their linear fits used to calculate crystallization age (released ^{40}Ar/^{36}Ar vs. ^{39}Ar/^{36}Ar in increasing temperature steps) tend to be relatively low (e.g. Harpel et al., 2004; Conway et al., 2016; Preece et al., 2018). Therefore, young ^{40}Ar/^{39}Ar ages are very susceptible to the decisions involved in the selection of steps included (or discarded) in the calculation of weighted mean plateau and isochron ages, and our exposure ages based on multiple samples provide more reliable results.

From the four sampled flows in this study with existing ^{40}Ar/^{39}Ar dates (Conway et al., 2016), two yield eruption ages that agree with the radiometric dates (Delta Corner and Tukino Slopes-b flows) and two not only outside the 2σ confidence interval of Conway et al. (2016) but older than the ^{40}Ar/^{39}Ar ages, the Lava Cascade (^{3}He$_{cos}$: 11.4 ± 2.3 ka and ^{40}Ar/^{39}Ar: 0.8 ± 5.6 ka, Mangatoetoenui flows), and the Taranaki Falls (^{3}He$_{cos}$: 14.6 ± 2.9 ka and ^{40}Ar/^{39}Ar: 8.8 ± 2.8 ka) flows. The imprecise nature of the radiometric age of the Lava Cascade flow and its weak isochron, together with the good agreement between our LC samples and the eruption ages we obtained for the Mangatoetoenui flows, leads us to conclude that our eruption age for the Lava Cascade flow is more robust than the date provided by Conway et al. (2016). Based on the good clustering of our results (Table 2), we suggest that our ^{3}He$_{cos}$ eruption age better represents the true eruption age of the Taranaki Falls flow. Additionally, our eruption age would explain the rootless nature of the flow (Townsend et al., 2017), as it is older than the flank collapse event that affected the northern summit area of Ruapehu at ca. 10.5 ka (Eaves et al., 2015) and, hence, the upper section of the Taranaki Falls flow (Fig. 6a).

Our results show, in general, good agreement with the lava flow eruption ages refined by Greve et al. (2016) at Ruapehu (Fig. 5). The only exception is the Taranaki Falls flow; the refinement by Greve et al. (2016) is based on the ^{40}Ar/^{39}Ar date of Conway et al. (2016), and, thus, it intrinsically agrees with this age and not with our results. Our ^{3}He$_{cos}$ eruption ages for the Delta Corner (7.8 ± 1.5 ka; INT 2σ 0.6 ka), Bruce Road (8.1 ± 2.1 ka; INT 2σ 1.5 ka), and Saddle Cone (9.9 ± 2.0 ka; INT 2σ 0.7 ka) flows match the respective age ranges of 8200–7900, 8800–8500, and 9850–8650 BP provided by Greve et al. (2016). Moreover, these results suggest that it is unlikely that P_3 errors have a significant impact on the accuracy of the eruption ages from this work, which is also supported by the good agreement of the local ^{3}He$_{cos}$ production rate calibration test by Eaves et al. (2015) with the worldwide mean production rate used in this study.

Eruption ages obtained for the Rangataua proximal and medial flows (13.6 ± 2.6 and 15.8 ± 3.0 ka, respectively) do not agree with a 12–10 ka constraint suggested by Price et al. (2012) based on tephra stratigraphy (using unpublished data). However, tephra correlation on Ruapehu is complex due to the large number of pyroclastic units emplaced at 20–11 ka and their broad geochemical ranges (Pardo et al., 2012a). Detailed studies (Donoghue et al., 2007) attempted to systematize tephra correlation in this area without success, indicating that the andesitic tephras are highly heterogeneous, displaying wide compositional fluctuations during short time intervals. Hence, our eruption ages are more robust than the estimate of 12–10 ka by Price et al. (2012). The other existing constraint for the Rangataua flows was given by a right lateral moraine of the Mangaehuehu valley dated at 11–14 ka by Eaves et al. (2019), which was thought to correspond in age to the left lateral moraine overlain by the RTm flow (Fig. 4d). Our eruption age of 15.8 ± 0.8 ka (INT 2σ; P_3 errors not considered as the moraines were dated using ^{3}He$_{cos}$) suggests that the moraine underlying the Rangataua flows is older than the dated right lateral moraine, rather than its equivalent.

Most of the flows dated in this study lack previous age constraints beyond estimations based on geochemical similarity and geographical proximity to lavas with ^{40}Ar/^{39}Ar dates. The eruption ages obtained for about half of these flows do not agree with these correlations (Fig. 5). Five of them (MN, MS, CTb, MF, and GR flows) yield ages younger than any of the dates informed for the units they were correlated to (i.e. Turoa, Makotuku, and Mangaehuehu members). This can be explained by a sampling bias of Conway et al. (2016) towards older flows that are more likely to have exposed their slowly cooled flow interiors (suitable for ^{40}Ar/^{39}Ar dating) due to their longer periods exposed to erosive processes and the presence of collapsed thick margins in the case of previously ice-impounded flows (Conway et al., 2015). PR and MA deposits are relatively isolated (Fig. 4a, b), so the previous geochemical correlations are weaker. The age previously assigned to the PR deposits (Table 1) was, unlike any other lava in this study, based on a correlation with a pyroclastic unit, adding another layer of uncertainty. Our results represent the first dates for lavas at the PR and MA sites and

Table 2. Results of helium isotope measurements and exposure ages by sample.

Sample	Latitude (S)	Longitude (E)	Elevation (m.s.l.)	Shielding factor	$^3He_{tot}$ $\pm1\sigma$ (10^6 at g^{-1})	$^4He_{tot}$ $\pm1\sigma$ (10^{10} at g^{-1})	Total $^3He/^4He$ (R/Ra)	$^3He_{cos}$ $\pm1\sigma$ (10^6 at g^{-1})	Exposure age $\pm1\sigma$ (ka)
DC – Delta Corner flow			**Tawhainui flows – Iwikau Member**						
DC-PD327	39.2346	175.5515	1600.4	0.999	2.82 ± 0.21	0.72 ± 0.05	283 ± 28	2.78 ± 0.21	7.52 ± 0.50
DC-PD329	39.2342	175.5509	1591.8	0.999	3.08 ± 0.23	0.98 ± 0.05	227 ± 20	3.03 ± 0.23	8.22 ± 0.56
DC-PD330	39.2341	175.5507	1590.3	0.999	2.89 ± 0.22	0.80 ± 0.05	260 ± 26	2.85 ± 0.22	7.72 ± 0.52
								Eruption age of DC: 7.8 ± 1.5 ka	
								INT 2σ: 0.6 ka	
BR – Bruce Road flow			**Tawhainui flows – Iwikau Member**						
BR-PD014	39.2201	175.5405	1360.0	0.999	2.33 ± 0.12	0.61 ± 0.05	277 ± 26	2.30 ± 0.13	7.37 ± 0.35
BR-PD016	39.2198	175.5379	1359.2	0.982	2.57 ± 0.14	1.45 ± 0.06	128 ± 9	2.49 ± 0.14	8.05 ± 0.41
BR-PD017	39.2190	175.5409	1332.6	0.998	2.47 ± 0.14	1.65 ± 0.08	108 ± 8	2.38 ± 0.15	7.75 ± 0.43
BR-PD018	39.2190	175.5411	1332.4	0.998	2.87 ± 0.16	1.14 ± 0.08	181 ± 16	2.81 ± 0.16	9.13 ± 0.50
								Eruption age of BR: 8.1 ± 2.1 ka	
								INT 2σ: 1.5 ka	
WG – Whakapapa Glacier flow			**Tawhainui flows – Iwikau Member**						
WG-PD325	39.2557	175.5551	2079.1	0.991	4.44 ± 0.22	0.91 ± 0.05	351 ± 26	4.40 ± 0.22	8.51 ± 0.39
WG-PD326	39.2556	175.5549	2066.7	0.995	3.67 ± 0.19	1.15 ± 0.07	230 ± 18	3.61 ± 0.19	7.13 ± 0.33
								Minimum eruption age of WG: 7.8 ± 2.4 ka	
								INT 2σ: 2.0 ka	
LC – Lava Cascade flow			**Mangatoetoenui flows – Iwikau Member**						
LC-PD254	39.2718	175.6052	1827.1	0.997	5.13 ± 0.36	1.22 ± 0.05	303 ± 25	5.07 ± 0.37	11.38 ± 0.75
LC-PD255	39.2718	175.6053	1826.6	0.997	5.01 ± 0.36	1.75 ± 0.06	206 ± 16	4.91 ± 0.36	11.14 ± 0.74
LC-PD256	39.2718	175.6053	1825.6	0.996	3.99 ± 0.29	1.46 ± 0.05	197 ± 16	3.91 ± 0.29	9.02 ± 0.62*
LC-PD257	39.2718	175.6053	1824.7	0.996	5.28 ± 0.33	0.89 ± 0.05	430 ± 37	5.24 ± 0.33	11.64 ± 0.68
								Eruption age of LC: 11.4 ± 2.3 ka	
								INT 2σ: 0.8 ka	
TSa – Tukino Slopes-a flow			**Mangatoetoenui flows – Iwikau Member**						
TSa-PD205	39.2761	175.6021	1905.1	0.983	3.98 ± 0.22	0.51 ± 0.10	570 ± 120	3.96 ± 0.23	8.74 ± 0.46
TSa-PD206	39.2761	175.6021	1905.9	0.997	4.41 ± 0.24	0.14 ± 0.08	2300 ± 1300	4.41 ± 0.24	9.51 ± 0.47
TSa-PD207	39.2761	175.6021	1905.5	0.997	4.61 ± 0.23	0.55 ± 0.06	600 ± 68	4.58 ± 0.23	9.85 ± 0.46
								Eruption age of TSa: 9.4 ± 1.8 ka	
								INT 2σ: 0.5 ka	
TSb – Tukino Slopes-b flow			**Mangatoetoenui flows – Iwikau Member**						
TSb-PD209	39.2815	175.5993	1932.5	0.997	5.06 ± 0.15	^{4}He below detection limit		5.06 ± 0.31	10.47 ± 0.59
TSb-PD210	39.2815	175.5992	1935.0	0.989	5.86 ± 0.28	1.41 ± 0.10	299 ± 25	5.78 ± 0.28	11.92 ± 0.54
TSb-PD211	39.2816	175.5993	1929.2	0.993	5.78 ± 0.28	0.80 ± 0.05	522 ± 44	5.74 ± 0.28	11.90 ± 0.55
								Eruption age of TSb: 11.5 ± 2.2 ka	
								INT 2σ: 0.6 ka	
TFt – Tukino Flats flow			**Mangatoetoenui flows – Iwikau Member**						
TFt-PD212	39.2726	175.6261	1521.2	0.994	2.71 ± 0.20	0.95 ± 0.06	206 ± 20	2.66 ± 0.21	7.71 ± 0.53
TFt-PD213	39.2726	175.6263	1522.0	0.998	3.86 ± 0.27	1.03 ± 0.04	270 ± 22	3.80 ± 0.28	10.77 ± 0.71
TFt-PD214	39.2723	175.6271	1506.4	0.988	2.47 ± 0.14	0.68 ± 0.06	263 ± 27	2.43 ± 0.14	7.28 ± 0.36
								Minimum eruption age of TFt: 8.6 ± 4.6 ka	
								INT 2σ: 4.3 ka	
TFa – Taranaki Falls flow			**Taranaki Falls flow – Iwikau Member**						
TFa-PD088	39.2067	175.5668	1308.2	0.999	4.65 ± 0.29	1.64 ± 0.06	204 ± 15	4.56 ± 0.29	14.62 ± 0.85
TFa-PD090	39.2060	175.5665	1302.8	0.996	4.38 ± 0.27	1.01 ± 0.05	312 ± 24	4.33 ± 0.27	14.23 ± 0.82
TFa-PD091	39.2059	175.5664	1288.2	0.999	4.69 ± 0.29	1.14 ± 0.04	296 ± 21	4.63 ± 0.29	15.04 ± 0.85
								Eruption age of TFa: 14.6 ± 2.9 ka	
								INT 2σ: 1.0 ka	
SCw – Saddle Cone flow (western lobe)			**Saddle Cone Member**						
SC-PD001	39.2143	175.6011	1439.0	0.998	3.85 ± 0.28	5.14 ± 0.12	54 ± 4	3.57 ± 0.31	10.53 ± 0.83
SC-PD002	39.2143	175.6010	1439.3	0.998	3.59 ± 0.26	3.03 ± 0.08	85 ± 7	3.43 ± 0.27	10.15 ± 0.75
SC-PD003	39.2146	175.5997	1443.3	0.998	3.45 ± 0.25	3.91 ± 0.09	63 ± 5	3.24 ± 0.27	9.54 ± 0.73
SCe – Saddle Cone flow (eastern lobe)									
SC-PD093	39.2115	175.6139	1308.18	0.993	2.97 ± 0.22	0.92 ± 0.05	233 ± 21	2.94 ± 0.22	9.64 ± 0.67
								Eruption age of SC: 9.9 ± 2.0 ka	
								INT 2σ: 0.7 ka	
WP – Waihohonu Plateau flow			**Saddle Cone Member**						
WP-PD007	39.2479	175.5882	1911.7	0.996	5.63 ± 0.23	2.06 ± 0.07	197 ± 11	5.55 ± 0.24	11.60 ± 0.45
WP-PD008	39.2479	175.5882	1912.1	0.995	5.22 ± 0.22	1.94 ± 0.03	194 ± 9	5.14 ± 0.23	10.81 ± 0.43
								Minimum eruption age of WP: 11.2 ± 2.2 ka	
								INT 2σ: 0.6 ka	

Table 2. Continued.

Sample	Latitude (S)	Longitude (E)	Elevation (m.s.l.)	Shielding factor	$^3He_{tot} \pm 1\sigma$ (10^6 at g^{-1})	$^4He_{tot} \pm 1\sigma$ (10^{10} at g^{-1})	Total $^3He/^4He$ (R/Ra)	$^3He_{cos} \pm 1\sigma$ (10^6 at g^{-1})	Exposure age $\pm 1\sigma$ (ka)
PR – Pinnacle Ridge spatter deposit			**Pinnacle Ridge Member**						
PR-PD083	39.2370	175.5672	1730.7	0.979	9.39 ± 0.44	6.56 ± 0.20	103 ± 6	9.03 ± 0.48	20.82 ± 1.00
PR-PD084	39.2386	175.5689	1860.9	0.988	9.42 ± 0.44	7.72 ± 0.24	88 ± 5	8.99 ± 0.49	19.04 ± 0.93
PR-PD085	39.2385	175.5688	1857.9	0.997	10.69 ± 0.49	5.84 ± 0.18	132 ± 7	10.37 ± 0.52	21.48 ± 1.00
									Eruption age of PR: 20.4 ± 4.0 ka
									INT 2σ: 1.1 ka
RTp – Rangataua proximal flow			**Rangataua Member**						
RTp-PD027	39.3140	175.5509	1831.4	0.997	6.38 ± 0.25	1.74 ± 0.08	264 ± 16	6.28 ± 0.26	13.88 ± 0.53
RTp-PD028	39.3140	175.5509	1833.1	0.996	5.73 ± 0.26	2.13 ± 0.12	194 ± 14	5.61 ± 0.26	12.41 ± 0.56
RTp-PD029	39.3140	175.5509	1832.9	0.996	6.42 ± 0.36	2.24 ± 0.18	206 ± 20	6.29 ± 0.37	13.88 ± 0.75
RTp-PD030	39.3143	175.5512	1816.4	0.988	6.45 ± 0.31	0.98 ± 0.06	474 ± 35	6.40 ± 0.31	14.35 ± 0.62
									Eruption age of RTp: 13.6 ± 2.6 ka
									INT 2σ: 0.6 ka
RTm – Rangataua medial flow			**Rangataua Member**						
RTm-PD045	39.3234	175.5520	1585.9	0.991	6.30 ± 0.38	1.83 ± 0.07	248 ± 17	6.20 ± 0.38	16.22 ± 0.91
RTm-PD046 (a)	39.3249	175.5508	1567.6	0.979	6.14 ± 0.25	0.74 ± 0.05	601 ± 48	6.10 ± 0.25	
RTm-PD046 (b)	39.3249	175.5508	1567.6	0.979	5.98 ± 0.30	0.98 ± 0.08	438 ± 43	5.93 ± 0.30	
RTm-PD046 mean	39.3249	175.5508	1567.6	0.979				6.04 ± 0.27	16.03 ± 0.64
RTm-PD047	39.3251	175.5503	1567.4	0.997	5.91 ± 0.29	1.13 ± 0.06	376 ± 28	5.85 ± 0.29	15.27 ± 0.68
RTm-PD048	39.3250	175.5503	1567.3	0.997	3.08 ± 0.16	1.64 ± 0.07	135 ± 9	2.99 ± 0.16	8.17 ± 0.40*
									Eruption age of RTm: 15.8 ± 3.0 ka
									INT 2σ: 0.8 ka
WT – Whakapapaiti flow			**Paretetaitonga Member**						
WT-PD073	39.2569	175.5428	1892.4	0.987	6.01 ± 0.28	0.35 ± 0.08	1230 ± 270	6.00 ± 0.28	12.78 ± 0.59
WT-PD074	39.2569	175.5428	1892.5	0.991	6.36 ± 0.26	0.73 ± 0.04	624 ± 39	6.33 ± 0.27	13.41 ± 0.54
WT-PD075	39.2560	175.5397	1785.0	0.990	6.06 ± 0.26	1.24 ± 0.05	352 ± 20	6.00 ± 0.27	13.74 ± 0.57
									Eruption age of WT: 13.3 ± 2.6 ka
									INT 2σ: 0.7 ka
MN – Mangaturuturu North flow			**Turoa Member**						
MN-PD217	39.2829	175.5322	1815.9	0.993	3.49 ± 0.24	0.30 ± 0.05	830 ± 150	3.48 ± 0.24	7.99 ± 0.50
MN-PD218	39.2829	175.5321	1813.9	0.993	3.82 ± 0.23	0.37 ± 0.04	739 ± 97	3.80 ± 0.23	8.85 ± 0.51
MN-PD219	39.2829	175.5321	1812.1	0.993	2.47 ± 0.19	0.42 ± 0.05	770 ± 200	2.46 ± 0.19	5.99 ± 0.39*
MN-PD220	39.2829	175.5322	1817.5	0.993	3.91 ± 0.25	0.77 ± 0.03	668 ± 89	3.89 ± 0.25	8.89 ± 0.54
MN-PD221	39.2829	175.5325	1822.8	0.993	3.30 ± 0.20	0.08 ± 0.04	1340 ± 400	3.29 ± 0.20	7.66 ± 0.42
									Eruption age of MN: 8.3 ± 1.6 ka
									INT 2σ: 0.5 ka
MS – Mangaturuturu South flow			**Turoa Member**						
MS-PD222	39.2845	175.5304	1750.6	0.954	2.58 ± 0.16	0.50 ± 0.04	371 ± 35	2.55 ± 0.16	6.67 ± 0.35
MS-PD223	39.2845	175.5305	1751.4	0.992	2.51 ± 0.17	0.12 ± 0.05	1560 ± 710	2.51 ± 0.17	6.32 ± 0.36
MS-PD224	39.2845	175.5305	1750.9	0.992	2.08 ± 0.16	0.40 ± 0.11	370 ± 100	2.06 ± 0.16	5.33 ± 0.37
									Minimum eruption age of MS: 6.1 ± 1.7 ka
									INT 2σ: 1.4 ka
CTa – Central Turoa-a flow			**Turoa Member**						
CTa-PD229	39.2958	175.5395	1924.0	0.996	6.57 ± 0.33	2.35 ± 0.09	201 ± 13	6.45 ± 0.34	13.24 ± 0.67
CTa-PD230	39.2959	175.5396	1925.1	0.996	6.93 ± 0.36	2.76 ± 0.11	181 ± 12	6.78 ± 0.37	13.89 ± 0.69
									Minimum eruption age of CTa: 13.6 ± 2.7 ka
									INT 2σ: 1.0 ka
CTb – Central Turoa-b flow			**Turoa Member**						
CTb-PD231	39.2998	175.5392	1877.5	0.996	2.11 ± 0.14	0.66 ± 0.06	230 ± 25	2.07 ± 0.14	4.93 ± 0.30*
CTb-PD232	39.3001	175.5390	1873.2	0.991	4.00 ± 0.24	0.74 ± 0.05	390 ± 33	3.96 ± 0.24	8.79 ± 0.49
CTb-PD233	39.3001	175.5390	1872.0	0.994	3.86 ± 0.25	0.93 ± 0.06	298 ± 28	3.81 ± 0.25	8.39 ± 0.52
CTb-PD234 (a)	39.3003	175.5391	1873.4	0.996	3.80 ± 0.24	0.90 ± 0.07	283 ± 28	3.75 ± 0.24	
CTb-PD234 (b)	39.3003	175.5391	1873.4	0.996	3.96 ± 0.27	0.60 ± 0.05	472 ± 50	3.93 ± 0.26	
CTb-PD234 mean	39.3003	175.5391	1873.4	0.996				3.85 ± 0.25	8.47 ± 0.51
									Eruption age of CTb: 8.6 ± 1.7 ka
									INT 2σ: 0.6 ka
TC – Turoa Cascades flow			**Turoa Member**						
TC-PD066	39.3014	175.5193	1533.2	0.997	4.13 ± 0.20	1.03 ± 0.06	288 ± 23	4.07 ± 0.21	11.37 ± 0.53*
TC-PD067	39.3015	175.5192	1533.6	0.997	5.24 ± 0.27	1.14 ± 0.05	331 ± 21	5.18 ± 0.26	14.09 ± 0.65
TC-PD068	39.3015	175.5192	1533.1	0.997	4.74 ± 0.23	1.09 ± 0.04	313 ± 18	4.68 ± 0.23	13.05 ± 0.62
TC-PD070	39.3012	175.5193	1528.0	0.997	4.89 ± 0.23	0.82 ± 0.04	431 ± 28	4.85 ± 0.23	13.27 ± 0.61
									Eruption age of TC: 13.4 ± 2.6 ka
									INT 2σ: 0.7 ka

Table 2. Continued.

Sample	Latitude (S)	Longitude (E)	Elevation (m.s.l.)	Shielding factor	$^3He_{tot} \pm 1\sigma$ (10^6 at g^{-1})	$^4He_{tot} \pm 1\sigma$ (10^{10} at g^{-1})	Total $^3He/^4He$ (R/Ra)	$^3He_{cos} \pm 1\sigma$ (10^6 at g^{-1})	Exposure age $\pm 1\sigma$ (ka)
MF – Makotuku Flats flow			**Makotuku Member**						
MF-PD061	39.3169	175.5143	1437.1	0.971	4.92 ± 0.26	1.93 ± 0.07	183 ± 12	4.82 ± 0.27	14.21 ± 0.73
MD-PD063	39.3168	175.5146	1434.8	0.991	4.00 ± 0.22	2.19 ± 0.09	131 ± 9	3.88 ± 0.23	11.45 ± 0.62
MF-PD064	39.3167	175.5146	1433.8	0.987	4.08 ± 0.22	1.65 ± 0.07	178 ± 12	3.99 ± 0.22	11.80 ± 0.61
MF-PD065	39.3167	175.5147	1433.3	0.988	4.47 ± 0.24	1.79 ± 0.08	180 ± 13	4.37 ± 0.25	12.80 ± 0.70
								Eruption age of MF: 12.6 ± 3.5 ka	
								INT 2σ: 2.5 ka	
NR – Ngā Rimutāmaka flow			**Makotuku Member**						
NR-PD053	39.3381	175.5873	1369.8	0.996	16.08 ± 0.67	2.46 ± 0.08	474 ± 25	16.05 ± 0.67	46.60 ± 2.12
NR-PD054	39.3384	175.5880	1372.9	1.000	15.34 ± 0.63	1.89 ± 0.07	582 ± 31	15.21 ± 0.64	43.38 ± 1.75
NR-PD055	39.3384	175.5879	1372.7	0.999	14.63 ± 0.62	1.79 ± 0.08	587 ± 35	14.52 ± 0.62	41.41 ± 1.53
NR-PD057	39.3384	175.5880	1372.6	0.995	14.80 ± 0.62	2.61 ± 0.10	408 ± 23	14.67 ± 0.63	42.11 ± 1.63
								Eruption age of NR: 42.9 ± 8.6 ka	
								INT 2σ: 1.7 ka	
MA – Makahikatoa flow			**Makotuku Member**						
MA-PD058	39.3125	175.6116	1594.8	0.996	20.03 ± 0.83	4.82 ± 0.15	299 ± 15	19.75 ± 0.84	48.96 ± 2.60
MA-PD059	39.3125	175.6116	1593.4	0.998	24.08 ± 1.18	9.56 ± 0.27	181 ± 10	23.58 ± 1.21	58.98 ± 2.84
								Minimum eruption age of MA: 54.0 ± 18.0 ka	
								INT 2σ: 14.2 ka	
GR – Girdlestone Ridge flow			**Mangaehuehu Member**						
GR-PD022 (Ol)	39.3072	175.5613	2148.0	0.996	7.88 ± 0.21	1.24 ± 0.10	457 ± 37	7.79 ± 0.21	14.02 ± 0.35
GR-PD023 (Ol)	39.3074	175.5615	2147.3	0.921	7.61 ± 0.49	1.19 ± 0.13	460 ± 59	7.54 ± 0.49	14.46 ± 0.85
GR-PD024 (Ol)	39.3074	175.5616	2145.4	0.990	6.19 ± 0.39	1.28 ± 0.07	348 ± 30	6.12 ± 0.39	11.11 ± 0.64*
GR-PD025 (Ol)	39.3078	175.5615	2128.1	0.993	3.61 ± 0.25	1.87 ± 0.10	139 ± 12	3.50 ± 0.25	6.81 ± 0.41*
								Minimum eruption age of GR: 14.2 ± 2.7 ka	
								INT 2σ: 0.6 ka	

$^3He_{cos}$ values were calculated using Eq. (3), with a magmatic $^3He/^4He$ of $5.9 \pm 2.6 \times 10^{-6}$ ($\sim 4.2 \pm 1.9$ Ra). Individual samples are informed with 1σ for reproducibility using the CREp online calculator. Summary eruption age uncertainties represent 2σ values including production rate errors. Internal (INT) 2σ errors do not include production rate errors. All analysed samples consisted of pure pyroxenes with the exception of the site GR where analysed crystals were olivines with subordinate pyroxenes. For complete data and corrections, see Table A3. Outliers are marked with a * after the calculated exposure age. Two aliquots were measured for samples RTm-PD046 and CTb-PD234 for which we calculated a weighted mean of the $^3He_{cos}$ as a sample summary.

indicate older eruption ages than suggested by geochemical correlations.

5.2 Inconsistency with previous unit classification

Most of the eruption ages measured in this study are consistent with the age and geochemical ranges of the units to which they were assigned by Townsend et al. (2017). Here, we discuss the results we obtained that do not agree with the existing classification.

- Donoghue et al. (1999) linked the Pinnacle Ridge spatter-fed lava with the Taurewa pyroclastic unit (ca. 10 ka) based on geochemistry and the concentric nature of the isopachs of the Taurewa deposits around the location of PR. Our results indicate that the Pinnacle Ridge deposit was emplaced at 20.4 ± 4.0 ka, during the LGM and ca. 10 kyr prior to the Taurewa eruptive event, which is consistent with the lack of preservation of a proximal vent, likely associated with a significant erosive period and the retreat of large ice masses. Hence, our eruption age for Pinnacle Ridge suggests that this unit should be included as part of the Mangawhero Formation (50–15 ka) instead of the Whakapapa Formation (< 15 ka).
- MF samples were taken from a large flow considered to be part of the Makotuku Member of the Mangawhero Formation (ca. 24–16 ka; Table 1) based on its geochemistry. Our results show that this lava flow erupted at 12.6 ± 3.5 ka, which suggests that, based on age criteria, it could be classified as part of the Whakapapa Formation (< 15 ka).
- Our NR site was mapped as part of the Makotuku Member in an area dominated by outcrops of Mangaehuehu lavas (Fig. 4d). Our eruption age of 42.9 ± 8.6 ka for this site, together with the geochemical similarity of the NR samples to Mangaehuehu lavas (47–40 ka; Conway et al., 2016; see Table 1), suggests that the sampled outcrop is part of the Mangaehuehu Member.
- The outcrop we collected the MA samples from has, due to its geochemical similarity, been considered part of the Makotuku Member. Two exposure ages indicate that the Makahikatoa flow was emplaced at, or prior to, 50 ka, suggesting that it was formed during the first eruptive stages of the Mangawhero or in the late stages of the Waihianoa Formation (see Table 1) with a geochemical signature common in lavas emplaced at 24–16 ka.
- Exposure ages of GR samples (previously mapped as part of the Mangaehuehu Member) suggest that this lava

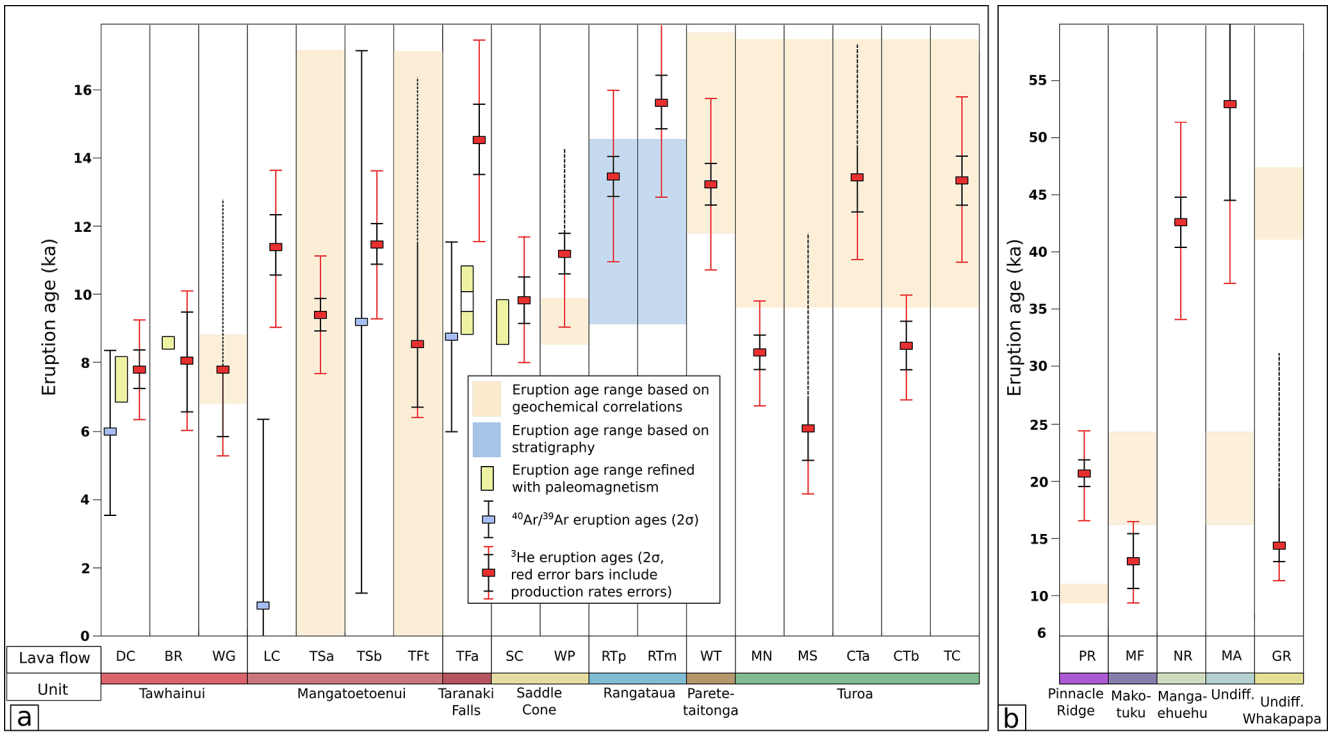

Figure 5. Comparison between eruption ages obtained in this study and previous chronological constraints of the sampled flows. Unit colours correspond to the colours in Fig. 1. **(a)** Lavas < 20 ka. **(b)** Lava flows that are, or were thought to be, older than 20 ka.

was emplaced during the last 15 kyr, which is inconsistent with it being part of the Mangawhero Formation. However, its geochemistry differentiates this outcrop from the rest of the Whakapapa lavas (Conway et al., 2016); thus it is likely to be part of a new member within the Whakapapa Formation.

– The results we obtained for flows from the Turoa Member indicate that lava was emplaced on Ruapehu's western flanks at ca. 15–12 ka (Turoa Cascades and Central Turoa-a flows as well as data from Conway et al., 2016) and, after a hiatus of ∼ 4 kyr, again at around 8 ka (Mangaturuturu North and Central Turoa-b flows). Thus, we suggest the extension of the younger limit of the Turoa Member to 8 ka. Similarly, the obtained eruption ages redefine the age limits of the Rangataua Member (17–12 ka), Saddle Cone Member (12–8.5 ka), Taranaki Falls flow (16–13 ka), and Mangatoetoenui flows (12–9 ka).

5.3 Postglacial effusive activity of Ruapehu

Our $^{3}He_{cos}$-based eruption ages allow two periods of enhanced effusive activity since the LGM to be identified on Ruapehu (17–12 ka, Fig. 6a and b; and 9–7.5 ka, Fig. 6e), during which lava emplacement on different areas of the volcano occurred nearly simultaneously.

Our results show that, during the last glacial termination (ca. 17–14 ka; Fig. 6a), effusive activity affected the southern (Rangataua medial and, likely, the immense distal Rangataua flows of > 1.5 km^3) and northern (Taranaki Falls flow) slopes of Ruapehu, suggesting that its southern and northern vents were active during this period. Radiometric dates published by Conway et al. (2016; see Table 1) suggest that, during this period, lava flows were also emplaced on Ruapehu's western (15.1 ± 2.4 ka, Turoa Member) and northwestern (14.8 ± 3.0 ka, Paretetaitonga Member) flanks. This period of generalized activity across Ruapehu continued until ca. 12 ka (Fig. 6b), with increasing intensity on the western flanks and decreasing intensity on the southern flanks. Eruption ages of the Whakapapaiti (13.3 ± 0.7 ka), Turoa Cascades (13.4 ± 0.7 ka), and Rangataua proximal (13.6 ± 0.6 ka) flows are nearly identical, indicating that lava emplacement occurred nearly simultaneously on different flanks of the volcanic edifice. In the Early Holocene (i.e. 12–10.5 ka, Fig. 6c), activity was focused on the east and northeast of the volcano, generating the first lavas of the Mangatoetoenui flows as well as lavas from satellite vents (Waihohonu Plateau flow). After a flank collapse that affected part of the northern edifice at ca. 10.5 ka (Eaves et al., 2015), lava flows continued to be emplaced on the eastern flanks from the northern vent and erupted from satellite vents on the northeast in short time lapses (< 2 kyr), generating the large Saddle Cone flow (Fig. 6d). The rate of lava produc-

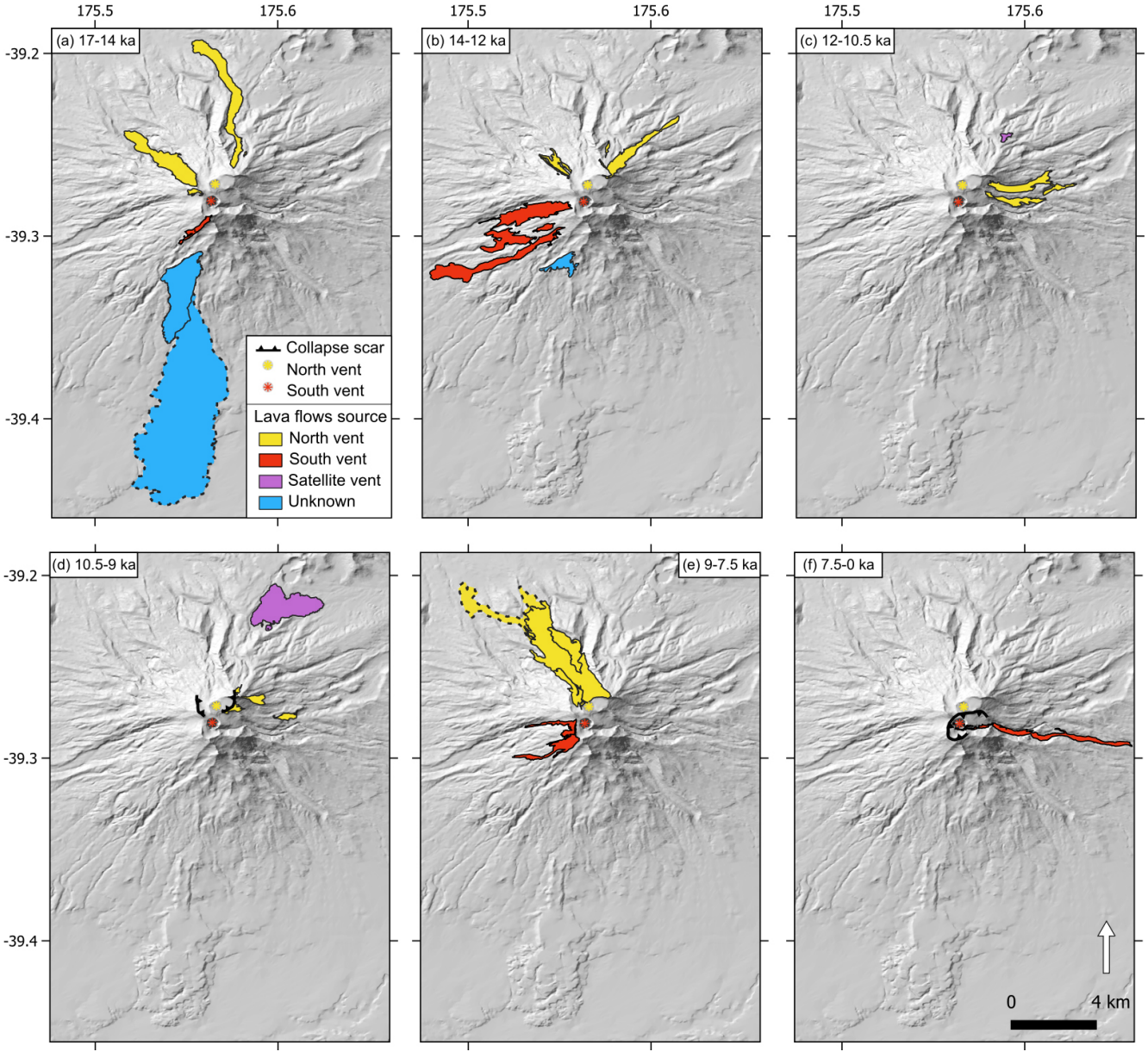

Figure 6. Lava flows emplaced at Ruapehu through time after the LGM. Collapse scars corresponds to flank collapse episodes at **(d)** 10.4–10.6 ka cal BP (Palmer and Neall, 1989; Eaves et al., 2015, Murimotu debris avalanche) and at **(f)** ca. 5.2 ka cal BP (Mangaio Formation, Donoghue, 1991; Donoghue and Neall, 2001). Lava flows with dotted boundaries in panels **(a)** and **(e)** have not been dated; their ages have been assigned based on geochemical and geomorphological similarities with dated flows.

tion (i.e. number of individual lava flows produced) between 9 and 7.5 ka (Fig. 6e) was likely to have been the highest in the last 20 kyr at Ruapehu. Our results suggest that, during this time, most of the flows forming the Tawhainui sequence on north Ruapehu were emplaced from the northern vent, filling a topographic low left by the flank collapse. At a similar time, the last lavas of the Turoa Member (Mangaturuturu North and Central Turoa-b flows) were erupted from the southern vent and flowed to the west of the edifice. Effusive activity then declined, and, after another episode of flank collapse that modified the topography surrounding the summit southern vent, lava flow emplacement was confined to the current outlet of Ruapehu's crater lake and flowed to the east (Whangaehu valley, Fig. 6f) at 2400–2050 BP (Greve et al., 2016).

Between ∼ 23 and ∼ 10 ka, Ruapehu produced at least five Plinian eruptions (as well as dozens of smaller explosive events) sourced from its northern vent (Pardo et al., 2012b). In contrast, effusive activity occurred from both the southern and northern vents until ∼ 8 ka. Lack of high-resolution

ages of the pyroclastic deposits, however, hinders our ability to precisely compare the timing of these events. After this period of enhanced volcanism (finishing at ∼ 10 ka for explosive events, Pardo et al., 2012b, and at ∼ 8 ka for effusive events), activity at Ruapehu decreased significantly in magnitude and was restricted to the southern vent. However, our data expose time intervals during the last 17 kyr when lavas have been emplaced from both of Ruapehu's summit vents, challenging the assumption that volcanic hazards should be expected from the southern vent but not from the northern vent (e.g. Keys and Green, 2010; Leonard et al., 2021).

5.4 Applicability of cosmogenic ^{3}He dating on stratovolcanoes

This study represents the first large-scale application of $^{3}He_{cos}$ as a dating tool for lava flows at stratovolcanoes. We provide $^{3}He_{cos}$-based eruption age constraints for 20 young lava flows at Ruapehu, contributing to a detailed lava flow eruptive history for Ruapehu during the last 20 kyr (Sect. 5.3). Our data have good intra-flow clustering, inter-flow consistency, and good agreement with previous chronological constraints, demonstrating that robust eruption ages can be obtained for lava flows using $^{3}He_{cos}$ not only for basaltic lavas (e.g. Kurz et al., 1990; Licciardi et al., 2007; Foeken et al., 2009; Marchetti et al., 2014; Medynski et al., 2015) but also for andesitic lavas at stratovolcanoes.

Analyses of our samples yielded low $^{4}He_{tot}$ values (likely influenced by repeated HF-leaching steps of the pyroxenes during sample preparation; Bromley et al., 2014) and low concentrations of radioactive elements (as expected from samples of intermediate compositions), which in turn resulted in small non-cosmogenic corrections and, added to analytical errors, small internal uncertainties in the obtained exposure ages. Like most other $^{3}He_{cos}$-based ages, however, the $^{3}He_{cos}$ production rate uncertainty makes the largest contribution to our errors, imparting an uncertainty of ∼ 10 % to all calculated ages, which points out that more high-quality calibration sites are required to reduce these uncertainties and improve the quality of ^{3}He-based exposure ages (Blard, 2021).

Considering these sources of uncertainties, our data show that the resolution of $^{3}He_{cos}$-based eruption ages can be higher than $^{40}Ar/^{39}Ar$ or K/Ar for young intermediate lavas (see Fig. 5). In older lava flows (> 20 ka), radiometric methods can resolve emplacement ages more precisely (e.g. Lanphere, 2000; Harpel et al., 2004; Conway et al., 2016), whereas cosmogenic exposure ages become less certain due to production rate errors. Consequently, cosmogenic nuclide exposure dating has the potential to yield better results compared to $^{40}Ar/^{39}Ar$ or K/Ar when dating post-LGM lava flows (e.g. Harpel et al., 2004; Parmelee et al., 2015; Conway et al., 2016; Alcalá-Reygosa et al., 2018) and offers a valid alternative to date older lavas when no radiometric dating method can be applied (e.g. the site NR from this study, whose age matches with higher-precision $^{40}Ar/^{39}Ar$ dates of geochemically similar lavas). Additionally, young lava flows are more likely to have original lava surfaces preserved as they were exposed to erosive and/or depositional processes for a relatively limited time. For the same reason, they are less likely to have exposed flow interiors needed for $^{40}Ar/^{39}Ar$ or K/Ar dating (Calvert and Lanphere, 2006; Fierstein et al., 2011), which makes $^{3}He_{cos}$ dating an ideal supplementary technique to radiometric methods when dating young pyroxene-bearing and olivine-bearing lavas at both basaltic volcanic areas and andesitic stratovolcanoes.

6 Conclusions

We analysed pyroxene-hosted and olivine-hosted $^{3}He_{cos}$ in 77 samples from 23 lava flows on Ruapehu volcano, Aotearoa / New Zealand, and obtained 16 eruption ages (between 7.8 ± 0.6 and 42.9 ± 1.7 ka; analytical 2σ) and 7 minimum eruption ages, refining the chronology of lava flow emplacement at Ruapehu in the last 20 kyr.

Our data expose that weak $^{40}Ar/^{39}Ar$ isochrons led to unreliable eruption ages for two postglacial lavas at Ruapehu and stress the necessity of robust age constraints when using paleomagnetism as an age-refining tool.

Our results show that effusive activity at Ruapehu occurred from different vents during the last 17 kyr, affecting various sectors of the volcanic edifice over short time intervals. Based on our observations, we propose that the number of effusive eruptions during the last 20 kyr peaked at 17–12 and 9–7.5 ka. This represents a significant contribution to the hazard database of Aotearoa / New Zealand and valuable data for investigating temporal links of volcanic activity in the Tāupo Volcanic Zone.

Cosmogenic nuclide exposure dating can provide greater detail on the recent effusive chronology of stratovolcanoes, filling the gap left by the low resolution and challenges in acquiring adequate samples for radiometric dating of young lava flows.

Appendix A

Table A1. Abbreviations list used for sampling sites and samples.

Abbreviation	Lava flow name	Area
BR	Bruce Road	North
CTa	Central Turoa-a	West
CTb	Central Turoa-b	West
DC	Delta Corner	North
GR	Girdlestone Ridge	South
LC	Lava Cascade	East
MA	Makahikatoa	Southeast
MF	Makotuku Flat	West
MN	Mangaturuturu North	West
MS	Mangaturuturu South	West
NR	Ngā Rimutāmaka	South
PR	Pinnacle Ridge	North
RTm	Rangataua medial	South
RTp	Rangataua proximal	South
SC	Saddle Cone	Northeast
SCw	Saddle Cone – western lobe	Northeast
SCe	Saddle Cone – eastern lobe	Northeast
TC	Turoa Cascades	West
TFa	Taranaki Falls	North
TFt	Tukino Flats	East
TSa	Tukino Slopes-a	East
TSb	Tukino Slopes-b	East
WG	Whakapapa Glacier	North
WP	Waihohonu Plateau	Northeast
WT	Whakapapaiti	Northwest

https://doi.org/10.5194/gchron-6-365-2024

Table A2. Normalized major and trace elements of bulk rock and analysed minerals for each sampled lava flow.

Bulk rock	Normalized wt %												Parts per million								
Site	SiO_2	Al_2O_3	Fe_2O_3	MnO	MgO	CaO	Na_2O	K_2O	TiO_2	P_2O_5	LOI	Maj_{tot}	Li	B	Cr	Co	Ni	Gd	Sm	U	Th
DC	57.01	15.88	8.23	0.13	5.37	7.42	3.14	1.40	0.68	0.18	0.56	99.26	17.9	20.0	85.19	26.68	45.59	2.69	2.75	1.08	4.04
BR	55.80	16.49	7.69	0.12	4.74	6.38	3.11	1.55	0.68	0.14	3.31	100.23	20.4	22.8	101.82	23.64	40.78	2.79	2.83	1.30	4.91
WG	54.87	16.02	9.25	0.13	5.34	6.59	2.92	1.41	0.72	0.14	2.62	99.46	17.6	20.1	91.32	26.95	45.80	2.75	2.75	1.13	4.36
LC	52.61	18.94	8.79	0.13	4.21	5.18	2.65	1.52	0.78	0.15	5.04	99.79	19.6	20.5	64.56	21.82	20.55	2.87	2.84	1.46	5.22
TSa	53.97	17.20	8.91	0.13	4.36	6.51	2.81	1.41	0.79	0.16	3.76	99.52	16.3	19.6	45.17	22.39	14.11	2.79	2.81	1.19	4.79
TSb	52.75	18.33	8.68	0.13	4.62	5.87	2.64	1.42	0.77	0.14	4.65	100.47	19.0	20.0	85.21	24.29	24.85	2.79	2.76	1.42	5.03
TFt	55.98	17.28	8.40	0.13	4.26	6.59	2.94	1.42	0.75	0.13	2.11	100.05	17.2	21.2	56.97	21.95	18.92	2.61	2.57	1.23	4.61
TFa	57.17	16.80	7.81	0.12	4.09	6.88	3.15	1.52	0.72	0.13	1.61	100.25	16.8	22.3	60.99	20.34	19.91	2.91	2.96	1.34	5.09
SC	56.76	16.48	7.88	0.12	4.64	7.02	3.07	1.52	0.72	0.15	1.63	99.87	21.3	21.7	86.23	23.75	31.36	2.77	2.81	1.32	4.92
WP	55.42	16.60	8.13	0.12	4.87	6.58	2.77	1.31	0.70	0.13	3.37	100.04	18.8	20.3	95.47	24.80	36.95	2.72	2.60	1.18	4.49
PR	58.59	16.12	6.78	0.10	4.42	5.69	3.04	1.79	0.65	0.14	2.68	100.29	22.5	21.9	183.67	20.39	53.61	2.57	2.50	1.45	5.50
RTp	56.56	17.39	7.60	0.12	3.37	5.35	3.15	1.74	0.75	0.15	3.84	99.83	19.2	23.9	36.93	16.88	12.67	3.00	3.11	1.49	5.91
RTm	56.64	16.82	7.67	0.12	3.57	5.72	3.15	1.69	0.75	0.21	3.67	99.53	18.6	23.4	40.90	17.75	13.20	3.15	3.17	1.53	6.03
WT	55.32	17.34	8.29	0.12	4.19	5.79	2.85	1.52	0.76	0.14	3.69	100.24	20.3	20.9	57.45	20.84	18.59	2.76	2.80	1.32	5.40
MN	53.66	17.72	8.07	0.12	5.01	6.09	2.93	1.47	0.66	0.13	4.14	100.44	19.2	22.5	93.87	25.17	47.08	2.42	2.41	1.34	4.86
MS	55.58	15.71	9.54	0.13	4.51	6.18	2.87	1.49	0.84	0.13	3.01	100.20	13.8	19.2	54.80	23.51	17.53	2.45	2.45	0.94	4.99
CTa	56.67	16.49	8.12	0.12	4.36	6.49	3.01	1.50	0.72	0.15	2.37	99.64	20.2	21.8	88.79	22.15	29.15	2.75	2.80	1.35	5.02
CTb	56.01	16.78	8.32	0.12	4.60	7.12	3.01	1.39	0.74	0.13	1.77	99.29	19.3	20.8	89.86	23.46	27.88	2.72	2.75	1.20	4.51
TC	56.18	16.49	8.44	0.13	4.60	7.03	3.06	1.48	0.78	0.14	1.66	99.90	17.3	20.0	71.52	22.48	18.63	2.96	2.95	1.22	4.71
MF	58.67	16.98	6.52	0.093	2.96	5.91	3.50	1.87	0.84	0.16	2.50	100.13	26.8	27.3	49.22	16.60	18.75	2.96	3.13	1.63	6.12
NR	57.92	14.71	6.81	0.11	6.24	5.96	2.96	1.85	0.73	0.19	2.53	99.77	29.7	23.4	308.14	25.08	109.34	3.14	3.25	1.74	6.50
MA	58.73	17.28	6.77	0.10	3.09	5.26	3.29	1.55	0.68	0.13	3.12	99.82	21.0	24.4	34.02	17.42	14.05	2.77	2.85	1.31	5.00
GR	55.76	15.21	7.40	0.12	6.09	6.77	2.80	1.35	0.66	0.14	3.71	100.13	20.4	20.7	215.77	26.79	73.65	2.71	2.78	1.14	4.50
Minerals																					
DC	52.11	1.58	20.53	0.41	22.11	4.08	0.09	<DL	0.31	<DL	−1.20	99.63	<2	10.7	285.89	98.63	187.40	1.07	0.78	0.01	0.040
BR	51.76	1.97	18.03	0.36	19.70	8.31	0.20	0.04	0.39	<DL	−0.76	99.55	<2	8.59	398.47	85.29	172.81	2.37	1.97	0.04	0.144
WG	51.71	1.61	20.15	0.39	21.71	4.76	0.10	<DL	0.34	<DL	−0.77	99.85	<2	12.8	371.23	92.22	182.44	1.38	1.08	0.01	0.048
LC	51.54	1.59	20.41	0.43	20.50	5.74	0.12	<DL	0.39	<DL	−0.71	99.32	<2	10.7	337.72	85.76	129.55	1.97	1.60	0.02	0.056
TSa	49.38	1.51	24.99	0.44	21.19	2.14	0.05	<DL	0.86	<DL	−0.57	99.83	<2	7.35	404.65	98.37	143.62	0.65	0.44	0.02	0.052
TSb	51.60	1.52	21.23	0.45	21.34	4.16	0.08	<DL	0.37	<DL	−0.76	100.32	<2	10.9	277.49	88.05	117.96	1.39	1.08	0.01	0.050
TFt	51.18	1.53	21.60	0.45	20.94	4.64	0.09	<DL	0.49	<DL	−0.90	99.54	<2	16.7	279.53	88.18	120.06	1.59	1.27	0.01	0.047
TFa	51.27	1.51	20.55	0.42	20.94	5.09	0.10	<DL	0.40	<DL	−0.28	99.10	<2	11.0	367.38	85.09	130.22	1.65	1.35	0.02	0.062
SC	51.41	1.91	19.70	0.39	19.54	7.18	0.18	0.04	0.42	<DL	−0.78	100.00	<2	9.17	394.61	80.89	127.03	2.56	2.07	0.05	0.185
WP	52.19	2.37	16.91	0.33	19.95	8.16	0.28	0.10	0.38	<DL	−0.67	99.86	<2	10.2	645.87	77.50	164.79	2.21	1.80	0.10	0.358
PR	51.05	2.01	20.06	0.39	20.02	6.31	0.13	<DL	0.41	<DL	−0.39	99.57	<2	31.0	632.12	83.14	163.52	1.94	1.54	0.03	0.141
RTp	51.08	1.50	22.65	0.43	21.53	3.04	0.07	<DL	0.49	<DL	−0.80	100.29	<2	5.71	405.44	91.30	153.24	1.06	0.80	0.01	0.049
RTm	51.38	1.46	23.10	0.44	21.71	2.91	0.06	<DL	0.47	<DL	−1.53	99.84	<2	7.48	321.50	91.05	135.00	1.07	0.82	0.01	0.045
WT	47.28	1.59	26.88	0.43	20.27	2.90	0.06	<DL	1.41	<DL	−0.82	99.76	<2	10.7	465.85	96.87	142.07	0.89	0.68	0.03	0.069
MN	52.02	1.51	21.69	0.43	22.68	2.47	0.06	<DL	0.31	<DL	−1.18	99.37	<2	13.4	269.95	102.76	196.34	0.66	0.46	0.01	0.040
MS	51.76	1.62	20.40	0.42	21.30	5.00	0.10	<DL	0.38	<DL	−0.97	99.36	<2	23.6	374.34	88.31	122.86	1.52	1.20	0.01	0.046
CTa	51.45	1.64	20.05	0.41	20.42	5.92	0.13	<DL	0.38	<DL	−0.40	99.89	<2	9.23	409.65	84.51	143.50	2.11	1.72	0.03	0.098
CTb	51.08	1.63	20.86	0.41	20.43	5.87	0.12	<DL	0.62	<DL	−1.03	99.35	<2	10.8	410.51	84.63	144.39	2.03	1.67	0.02	0.065
TC	51.56	1.62	20.37	0.41	21.10	5.02	0.10	<DL	0.35	<DL	−0.53	100.21	<2	8.01	391.62	88.11	124.68	1.51	1.19	0.01	0.046
MF	50.94	1.66	22.07	0.39	21.93	3.35	0.07	<DL	0.82	<DL	−1.22	99.65	<2	13.6	475.60	95.40	181.14	0.94	0.73	0.02	0.058
NR	52.64	1.95	16.10	0.28	22.62	6.82	0.15	<DL	0.35	<DL	−0.90	99.71	<2	11.7	1184.21	83.92	352.04	1.56	1.27	0.02	0.042
MA	49.70	2.03	22.77	0.39	21.09	3.88	0.08	<DL	0.89	<DL	−0.83	99.44	<2	17.7	332.48	92.02	106.83	0.88	0.64	0.02	0.081
GR	54.07	1.52	13.92	0.27	27.48	2.89	0.05	<DL	0.19	<DL	−0.39	99.30	<5	6.22	1649.09	87.13	360.96	0.36	0.26	<DL	0.022

Detection limits (DL) are at a 0.03 wt % for K_2O; 0.10 wt % for P_2O_5; 2 ppm for B; and 0.01 ppm for U.

Table A3. Sample data used to compute exposure ages.

Sample	Latitude (S)	Longitude (E)	Elevation (m.s.l.)	Surface dip (°)	Dip direction (°)	Shielding factor	Density (g cm^{-3})	Thickness (cm)	P_{nuc} (10^2 at g^{-1} yr^{-1})	Closure age (Ma)	He_{nuc} (at)	P_3 (at g^{-1} yr^{-1})	P_4 (10^5 at g^{-1} yr^{-1})	R factor
SC-PD001	39.2143	175.6011	1439.0	–	–	0.998	1.89	3.6	406	0.010	406	231.22	3.13	0.9932
SC-PD002	39.2143	175.6010	1439.3	–	–	0.998	2.01	3.2				245.83		0.9932
SC-PD003	39.2146	175.5997	1443.3	–	–	0.998	2.01	2.4				245.86		0.9932
WP-PD007	39.2479	175.5882	1911.7	10	190	0.996	2.13	3.3	414	0.010	415	487.90	6.08	0.9906
WP 008	39.2479	175.5882	1912.1	18	30	0.995	2.06	3.0				487.90		0.9906
BR-PD014	39.2201	175.5406	1360.0	–	–	0.999	2.15	2.7	565	0.010	565	317.93	0.75	0.9982
BR-PD016	39.2198	175.5379	1359.2	28	55	0.981	2.32	2.6				320.37		0.9982
BR-PD017	39.2190	175.5409	1332.6	–	–	0.998	2.25	2.7				313.04		0.9982
BR-PD018	39.2190	175.5411	1332.4	–	–	0.998	2.15	4.3				317.93		0.9982
GR-PD022	39.3072	175.5613	2148.0	–	–	0.996	2.15	2.7	254	0.020	508	589.39	0.44	0.9994
GR-PD023	39.3072	175.5615	2147.2	45	180	0.921	2.24	4.5				584.50		0.9994
GR-PD024	39.3074	175.5616	2145.4	–	–	0.990	2.18	4.6				574.72		0.9994
GR-PD025	39.3078	175.5615	2128.1	–	–	0.993	2.80	4.7				539.25		0.9994
RT-PD027	39.3140	175.5509	1831.4	–	–	0.997	1.84*	5.5	296	0.015	444	468.33	0.74	0.9988
RT-PD028	39.3140	175.5509	1833.1	–	–	0.996	1.79	5.3				467.11		0.9988
RT 029	39.3140	175.5509	1832.9	–	–	0.996	1.84*	5.3				469.56		0.9988
RT-PD030	39.3143	175.5512	1816.4	20	230	0.988	1.89	5.1				465.89		0.9988
RT-PD045	39.3234	175.5520	1585.9	20	80	0.991	2.80	4.2	401	0.015	601	399.86	0.75	0.9986
RT-PD046	39.3249	175.5508	1567.6	29	145	0.979	2.07	3.6				393.74		0.9986
RT-PD047	39.3251	175.5503	1567.4	–	–	0.997	2.27	3.0				392.52		0.9986
RT-PD048	39.3250	175.5503	1567.3	–	–	0.997	2.19	3.4				374.18		0.9985
NR-PD053	39.3381	175.5873	1369.8	15	3	0.996	2.39	4.8	654	0.045	2944	359.50	1.01	0.9979
NR-PD054	39.3384	175.5880	1372.9	–	–	1.000	2.06	4.2				360.73		0.9979
NR-PD055	39.3384	175.5879	1372.5	–	–	0.999	2.15	3.2				358.28		0.9979
NR-PD057	39.3384	175.5880	1372.6	–	–	0.995	2.47	3.5				359.50		0.9979
MA-PD058	39.3125	175.6116	1570.7	14	190	0.996	2.45	2.9	818	0.050	4089	414.53	1.29	0.9977
MA-PD059	39.3125	175.6116	1569.3	–	–	0.998	2.21	3.20				408.42		0.9976
MF-PD061	39.3169	175.5143	1437.0	–	–	0.971	2.15	3.0	729	0.013	948	353.39	1.14	0.9975
MF-PD063	39.3168	175.5146	1434.8	–	–	0.991	1.81	3.8				348.50		0.9975
MF-PD064	39.3167	175.5146	1433.8	–	–	0.987	1.95	3.6				349.72		0.9975
MF-PD065	39.3167	175.5147	1433.3	11	180	0.988	1.80	2.6				350.94		0.9975
TC-PD066	39.3014	175.5193	1533.2	–	–	0.997	2.17	6.2	292	0.013	380	375.40	7.59	0.9985
TC-PD067	39.3015	175.5192	1533.6	–	–	0.997	2.11	4.5				379.07		0.9985
TC-PD068	39.3015	175.5192	1533.1	–	–	0.997	2.15	7.4				377.85		0.9985
TC-PD070	39.3012	175.5193	1528.0	–	–	0.997	1.99	4.3				376.62		0.9985
WT-PD073	39.2569	175.5428	1892.4	20	260	0.987	2.09	3.5	493	0.013	641	468.33	0.77	0.9984
WT-PD074	39.2569	175.5428	1892.1	–	–	0.988	2.22	3.8				471.99		0.9984
WT-PD075	39.2560	175.5397	1891.2	–	–	0.997	2.18	3.3				471.99		0.9984
PR-PD083	39.2370	175.5672	1730.7	16	310	0.979	2.28	3.5	1557	0.020	3115	453.66	2.11	0.9965
PR-PD084	39.2386	175.5689	1860.9	24	180	0.988	2.18	4.7				492.79		0.9968
PR-PD085	39.2385	175.5688	1857.9	16	330	0.997	2.12	4.3				497.68		0.9968
TFa-PD088	39.2067	175.5668	1308.2	–	–	0.999	2.39	3.8	513	0.015	769	321.60	1.17	0.9973
TFa-PD090	39.2060	175.5665	1290.4	16	90	0.996	2.31	5.0				316.71		0.9972
TFa-PD091	39.2059	175.5664	1288.2	–	–	0.999	2.23	4.2				317.93		0.9972
SC-PD093	39.2115	175.6139	1308.2	17	40	0.993	2.30	2.6	537	0.010	537	313.04	3.71	0.9911
TSa-PD205	39.2761	175.6021	1905.0	–	–	0.983	2.12	5.6	305	0.010	305	476.89	1.05	0.9983
TSa-PD206	39.2761	175.6021	1905.9	–	–	0.997	2.21	4.8				480.56		0.9984
TSa-PD207	39.2761	175.6021	1905.5	–	–	0.997	2.37	4.2				481.78		0.9984
TSb-PD209	39.2815	175.5993	1932.5	–	–	0.997	2.20*	2.4	506	0.010	506	494.01	0.75	0.9989
TSb-PD210	39.2815	175.5992	1935.0	17	90	0.989	2.14	2.9				500.13		0.9988
TSb-PD211	39.2816	175.5993	1929.2	20	110	0.993	2.26	3.7				497.68		0.9988
TFt-PD212	39.2726	175.6261	1521.2	–	–	0.994	2.07	5.9	703	0.010	703	359.50	0.76	0.9984
TFt-PD213	39.2726	175.6263	1522.0	10	40	0.998	2.14	6.5				369.29		0.9985
TFt-PD214	39.2723	175.6271	1506.4	–	–	0.988	2.23	6.5				353.39		0.9984
MN-PD217	39.2829	175.5322	1815.9	–	–	0.993	2.11	2.6	623	0.008	498	446.32	0.65	0.9989
MN-PD218	39.2829	175.5321	1813.9	13	220	0.993	2.24	5.2				448.77		0.9989
MN-PD219	39.2829	175.5321	1812.1	–	–	0.993	2.22	4.0				425.53		0.9988
MN-PD220	39.2829	175.5322	1817.5	–	–	0.993	2.06	3.2				449.99		0.9989
MN-PD221	39.2829	175.5325	1822.8	–	–	0.993	2.20	4.0				446.32		0.9989
MS-PD222	39.2845	175.5304	1750.6	36	170	0.955	2.23	5.0	901	0.010	901	414.53	0.76	0.9986
MS-PD223	39.2845	175.5305	1751.4	–	–	0.992	2.41	4.0				412.08		0.9986
MS-PD224	39.2845	175.53005	1750.9	–	–	0.992	2.33	4.1				401.08		0.9986
CTa-PD229	39.2958	175.5395	1924.0	7	300	0.996	1.96	3.2	415	0.015	623	498.90	1.81	0.9972
CTa-PD230	39.2959	175.5396	1925.1	–	–	0.996	2.21	2.9				500.13		0.9973
CTb-PD231	39.2998	175.5392	1877.5	–	–	0.996	2.22	3.4	439	0.008	351	432.87	1.26	0.9978
CTb-PD232	39.3001	175.5390	1873.2	20	190	0.991	2.14	4.1				467.11		0.9979
CTb-PD233	39.3001	175.5390	1872.0	15	240	0.994	2.17*	2.8				465.89		0.9979
CTb-PD234	39.3003	175.5391	1873.4	–	–	0.996	2.15	3.2				467.11		0.9979
LC-PD254	39.2718	175.6052	1827.1	–	–	0.997	2.01	5.4	506	0.010	506	462.22	1.18	0.9981
LC-PD255	39.2718	175.6053	1826.6	–	–	0.997	2.07	6.4				461.00		0.9981
LC-PD256	39.2718	175.6053	1825.6	–	–	0.996	2.08	6.0				452.44		0.9980
LC-PD257	39.2718	175.6053	1824.7	16	330	0.996	2.05	3.7				462.22		0.9981
WG-PD325	39.2557	175.5551	2079.1	21	357	0.991	2.25	4.0	329	0.008	264	536.81	2.45	0.9966
WG-PD326	39.2556	175.5549	2066.7	–	–	0.995	2.30	3.2				520.91		0.9965
DC-PD327	39.2346	175.5515	1600.4	–	–	0.999	2.22	3.5	401	0.008	321	379.07	0.67	0.9987
DC-PD329	39.2342	175.5509	1591.8	–	–	0.999	2.37	4.3				380.29		0.9987
DC-PD330	39.2341	175.5507	1590.3	–	–	0.999	2.21	3.4				377.85		0.9987

Density measures were obtained with the hydrostatic method. Density values marked with * were calculated by averaging the densities of other samples from the same site. P_{nuc}, Closure age, He_{nuc}, and P_4 values are considered equal for all samples of the same flow.

Data availability. All used data are available in the Supplement file S4 and Appendix Table A2.

Supplement. The supplement related to this article is available online at: https://doi.org/10.5194/gchron-6-365-2024-supplement.

Author contributions. PD carried out field sampling, mineral separation, He isotope measurements, data processing and interpretation, and manuscript writing. SRE assisted with sampling, data processing, and manuscript revision. BMK handled the project supervision, obtained resources, and reviewed the manuscript. PHB helped with methodology, data analysis, and manuscript revision. ARLN reviewed and edited the manuscript. GSL helped with resources and data interpretation. DBT assisted with data interpretation. JWC helped with manuscript revision. CEC helped with data interpretation. SB assisted with mineral separation. GF, LZ, and BT helped with He isotope measurements.

Competing interests. The contact author has declared that none of the authors has any competing interests.

Disclaimer. Publisher's note: Copernicus Publications remains neutral with regard to jurisdictional claims made in the text, published maps, institutional affiliations, or any other geographical representation in this paper. While Copernicus Publications makes every effort to include appropriate place names, the final responsibility lies with the authors.

Acknowledgements. We would like to acknowledge Ngāti Rangi, Uenuku, and Ngāti Tūwharetoa iwi; *tangata whenua* and guardians of Ruapehu. We are grateful to Mark Kurz, David Marchetti, and Eric Portenga, whose comments as referees significantly improved the quality of this paper. We would like to thank New Zealand's Department of Conservation for sampling permission. We would also like to thank Amy Dreyer, Gilles Seropian, and Alexander James Marshall for their assistance in the field; Hollei Gabrielsen for her advice on Māori subjects and aid with the permit process; Chris Grimshaw for help with laboratory procedures; and Mark Henson and Nigel Seebeck for their help in the Tukino Access Road ford.

Financial support. This research has been supported by the Resilience to Nature's Challenges (RNC) volcano program (grant no. GNS-RNC047), the SAAFE scholarship 2022 from the Australian Institute of Nuclear Science and Engineering (AINSE), the Mason Trust (SEE, University of Canterbury), the Wellman Research Award 2022 (Royal Society of New Zealand), and the Tongariro Memorial Award 2022 (the Tongariro Natural History Society).

Review statement. This paper was edited by Marissa Tremblay and reviewed by Mark Kurz, David Marchetti, and Eric Portenga.

References

Ackert, R. P., Singer, B. S., Guillou, H., Kaplan, M. R., and Kurz, M. D.: Long-term cosmogenic ^{3}He production rates from ^{40}Ar/^{39}Ar and K-Ar dated Patagonian lava flows at 47° S, Earth Planet. Sci. Lett., 210, 119–136, https://doi.org/10.1016/S0012-821X(03)00134-1, 2003.

Alcalá-Reygosa, J., Palacios, D., Schimmelpfennig, I., Vázquez-Selem, L., García-Sancho, L., Franco-Ramos, O., Villanueva, J., Zamorano, J. J., Aumaître, G., Bourlès, D., and Keddadouche, K.: Dating late Holocene lava flows in Pico de Orizaba (Mexico) by means of in situ-produced cosmogenic ^{36}Cl, lichenometry and dendrochronology, Quat. Geochronol., 47, 93–106, https://doi.org/10.1016/j.quageo.2018.05.011, 2018.

Anderson, S. W., Krinsley, D. H., and Fink, J. H.: Criteria for recognition of constructional silicic lava flow surfaces, Earth Surf. Proc. Land., 19, 531–541, https://doi.org/10.1002/esp.3290190606, 1994.

Balco, G., Stone, J. O., Lifton, N. A., and Dunai, T. J.: A complete and easily accessible means of calculating surface exposure ages or erosion rates from ^{10}Be and ^{26}Al measurements, Quat. Geochronol., 3, 174–195, https://doi.org/10.1016/j.quageo.2007.12.001, 2008.

Barrell, D. J.: Quaternary Glaciers of New Zealand, in: Developments in Quaternary Sciences, 15 edn., chap. 75, Elsevier, 1047–1064, https://doi.org/10.1016/B978-0-444-53447-7.00075-1, 2011.

Barrell, D. J. A., Almond, P. C., Vandergoes, M. J., Lowe, D. J., and Newnham, R. M.: A composite pollen-based stratotype for inter-regional evaluation of climatic events in New Zealand over the past 30,000 years (NZ-INTIMATE project), Quaternary Sci. Rev., 74, 4–20, https://doi.org/10.1016/j.quascirev.2013.04.002, 2013.

Blard, P.-H.: Cosmogenic ^{3}He in terrestrial rocks: A review, Chem. Geol., 586, 120543, https://doi.org/10.1016/j.chemgeo.2021.120543, 2021.

Blard, P.-H. and Farley, K. A.: The influence of radiogenic ^{4}He on cosmogenic ^{3}He determinations in volcanic olivine and pyroxene, Earth Planet. Sci. Lett., 276, 20–29, https://doi.org/10.1016/j.epsl.2008.09.003, 2008.

Blard, P. H., Pik, R., Lavé, J., Bourlès, D., Burnard, P. G., Yokochi, R., Marty, B., and Trusdell, F.: Cosmogenic ^{3}He production rates revisited from evidences of grain size dependent release of matrix-sited helium, Earth Planet. Sci. Lett., 247, 222–234, https://doi.org/10.1016/j.epsl.2006.05.012, 2006.

Blard, P. H., Lavé, J., Pik, R., Wagnon, P., and Bourlès, D.: Persistence of full glacial conditions in the central Pacific until 15,000 years ago, Nature, 449, 591–594, https://doi.org/10.1038/nature06142, 2007.

Blard, P.-H., Braucher, R., Lavé, J., and Bourlès, D.: Cosmogenic ^{10}Be production rate calibrated against ^{3}He in the high Tropical Andes (3800–4900 m , 20–22° S), Earth Planet. Sci. Lett., 382, 140–149, https://doi.org/10.1016/j.epsl.2013.09.010, 2013.

Blard, P.-H., Balco, G., Burnard, P. G., Farley, K. A., Fenton, C. R., Friedrich, R., Jull, A. J., Niedermann, S., Pik, R., Schaefer, J. M., Scott, E. M., Shuster, D. L., Stuart, F. M., Stute, M., Tibari, B., Winckler, G., and Zimmermann, L.: An inter-laboratory comparison of cosmogenic ^{3}He and radiogenic ^{4}He in

the CRONUS-P pyroxene standard, Quat. Geochronol., 26, 11–19, https://doi.org/10.1016/j.quageo.2014.08.004, 2015.

Bromley, G. R., Winckler, G., Schaefer, J. M., Kaplan, M. R., Licht, K. J., and Hall, B. L.: Pyroxene separation by HF leaching and its impact on helium surface-exposure dating, Quat. Geochronol., 23, 1–8, https://doi.org/10.1016/j.quageo.2014.04.003, 2014.

Buchanan-Banks, J. M., Lockwood, J. P., and Rubin, M.: Radiocarbon dates for lava flows from northeast rift zone of Mauna Loa volcano, Hilo 7 1/2′ Quadrangle, island of Hawaii, Radiocarbon, 31, 179–186, 1989.

Calvert, A. T. and Lanphere, M. A.: Argon geochronology of Kilauea's early submarine history, J. Volcanol. Geoth. Res., 151, 1–18, https://doi.org/10.1016/j.jvolgeores.2005.07.023, 2006.

Calvert, A. T., Fierstein, J., and Hildreth, W.: Eruptive history of Middle Sister, Oregon Cascades, USA-Product of a late Pleistocene eruptive episode, Geosphere, 14, 2118–2139, https://doi.org/10.1130/GES01638.1, 2018.

Carignan, J., Hild, P., Mevelle, G., Morel, J., and Yeghicheyan, D.: Routine analyses of trace elements in geological samples using flow injection and low pressure on-line liquid chromatography coupled to ICP-MS: A study of geochemical reference materials BR, DR-N, UB-N, AN-G and GH, Geostandard. Newslett., 25, 187–198, https://doi.org/10.1111/j.1751-908x.2001.tb00595.x, 2001.

Cerling, T. E. and Craig, H.: Geomorphology and in-situ cosmogenic isotopes, Annu. Rev. Earth Pl. Sc., 273–317, 1994.

Clay, P. L., Busemann, H., Sherlock, S. C., Barry, T. L., Kelley, S. P., and McGarvie, D. W.: ^{40}Ar/^{39}Ar ages and residual volatile contents in degassed subaerial and subglacial glassy volcanic rocks from Iceland, Chem. Geol., 403, 99–110, https://doi.org/10.1016/j.chemgeo.2015.02.041, 2015.

Coble, M. A., Grove, M., and Calvert, A. T.: Calibration of Nu-Instruments Noblesse multicollector mass spectrometers for argon isotopic measurements using a newly developed reference gas, Chem. Geol., 290, 75–87, https://doi.org/10.1016/j.chemgeo.2011.09.003, 2011.

Cole, J. W. and Lewis, K. B.: Evolution of the Taupo-Hikurangi subduction system, Tectonophysics, 72, 1–21, https://doi.org/10.1016/0040-1951(81)90084-6, 1981.

Connor, C., Bebbington, M., and Marzocchi, W.: Probabilistic Volcanic Hazard Assessment, Elsevier Inc., second edn., ISBN 9780123859389, https://doi.org/10.1016/b978-0-12-385938-9.00051-1, 2015.

Conway, C. E.: Studies on the Glaciovolcanic and Magmatic Evolution of Ruapehu Volcano, New Zealand, PhD thesis, Victoria University of Wellington, https://researcharchive.vuw.ac.nz/handle/10063/5152 (last access: 25 May 2024), 2016.

Conway, C. E., Townsend, D. B., Leonard, G. S., Wilson, C. J., Calvert, A. T., and Gamble, J. A.: Lava-ice interaction on a large composite volcano: a case study from Ruapehu, New Zealand, B. Volcanol., 77, 21, https://doi.org/10.1007/s00445-015-0906-2, 2015.

Conway, C. E., Leonard, G. S., Townsend, D. B., Calvert, A. T., Wilson, C. J., Gamble, J. A., Eaves, S. R., Pure, L. R., Leonard, G. S., Townsend, D. B., Wilson, C. J., Calvert, A. T., Cole, R. P., Conway, C. E., Gamble, J. A., and Smith, T. B.: A high-resolution ^{40}Ar/^{39}Ar lava chronology and edifice construction history for Ruapehu volcano, New Zealand, J. Volcanol. Geoth. Res., 327, 152–179, https://doi.org/10.1016/j.jvolgeores.2016.07.006, 2016.

Delunel, R., Blard, P.-H., Martin, L. C., Nomade, S., and Schlunegger, F.: Long term low latitude and high elevation cosmogenic ^{3}He production rate inferred from a 107 ka-old lava flow in northern Chile; 22° S–3400 m a.s.l., Geochim. Cosmochim. Ac., 184, 71–87, https://doi.org/10.1016/j.gca.2016.04.023, 2016.

Donoghue, S. L.: Late quaternary volcanic stratigraphy of the southeastern sector of the Mount Ruapehu ring plain New Zealand, PhD thesis, Massey University, https://mro.massey.ac.nz/items/516a0d80-eda3-4a7e-a495-2e13fcb7821c (last access: 25 May 2024), 1991.

Donoghue, S. L. and Neall, V. E.: Late Quaternary constructional history of the southeastern Ruapehu ring plain, New Zealand, New Zeal. J. Geol. Geop., 44, 439–466, https://doi.org/10.1080/00288306.2001.9514949, 2001.

Donoghue, S. L., Neall, V. E., and Palmer, A. S.: Stratigraphy and chronology of late quaternary andesitic tephra deposits, Tongariro Volcanic Centre, New Zealand, J. Roy. Soc. New Zeal., 25, 115–206, https://doi.org/10.1080/03014223.1995.9517487, 1995.

Donoghue, S. L., Stewart, R. B., Neall, V. E., Lecointre, J., Price, R., Palmer, A. S., McClelland, E., and Hobson, K.: The Taurewa Eruptive Episode: Evidence for climactic eruptions at Ruapehu volcano, New Zealand, B. Volcanol., 61, 223–240, https://doi.org/10.1007/s004450050273, 1999.

Donoghue, S. L., Vallance, J. W., Smith, I. E., and Stewart, R. B.: Using geochemistry as a tool for correlating proximal andesitic tephra: case studies from Mt Rainier (USA) and MT Ruapehu (New Zealand), J. Quaternary Sci., 22, 395–410, https://doi.org/10.1002/jqs.1065, 2007.

Dostal, J., Dupuy, C., Carron, J. P., Le Guen de Kerneizon, M., and Maury, R. C.: Partition coefficients of trace elements: Application to volcanic rocks of St. Vincent, West Indies, Geochim. Cosmochim. Ac., 47, 525–533, https://doi.org/10.1016/0016-7037(83)90275-2, 1983.

Dunai, T. J.: Cosmogenic Nuclides. Pinciples, Concepts and Application in the Earth Surface Sciences, Cambridge University Press, ISBN 9780521873802, 2010.

Dunn, T. and Sen, C.: Mineral/matrix partition coefficients for orthopyroxene, plagioclase, and olivine in basaltic to andesitic systems: A combined analytical and experimental study, Geochim. Cosmochim. Ac., 58, 717–733, https://doi.org/10.1016/0016-7037(94)90501-0, 1994.

Eaves, S. R. and Brook, M. S.: Glaciers and glaciation of North Island, New Zealand, New Zeal. J. Geol. Geop., 64, 1–20, https://doi.org/10.1080/00288306.2020.1811354, 2021.

Eaves, S. R., Winckler, G., Schaefer, J. J. M., Vandergoes, M. J., Alloway, B. V., Mackintosh, A. N., Townsend, D. B., Ryan, M. T., and Li, X.: A test of the cosmogenic ^{3}He production rate in the south-west Pacific (39° S), J. Quaternary Sci., 30, 79–87, https://doi.org/10.1002/jqs.2760, 2015.

Eaves, S. R., Mackintosh, A. N., Anderson, B. M., Doughty, A. M., Townsend, D. B., Conway, C. E., Winckler, G., Schaefer, J. M., Leonard, G. S., and Calvert, A. T.: The Last Glacial Maximum in the central North Island, New Zealand: palaeoclimate inferences from glacier modelling, Clim. Past, 12, 943–960, https://doi.org/10.5194/cp-12-943-2016, 2016a.

Eaves, S. R., Mackintosh, A. N., Winckler, G., Schaefer, J. M., Alloway, B. V., and Townsend, D. B.: A cosmogenic ^{3}He chronology of late Quaternary glacier fluctuations in North Island, New Zealand (39° S), Quaternary Sci. Rev., 132, 40–56, https://doi.org/10.1016/j.quascirev.2015.11.004, 2016b.

Eaves, S. R., Winckler, G., Mackintosh, A. N., Schaefer, J. M., Townsend, D. B., Doughty, A. M., Jones, R. S., and Leonard, G. S.: Late-glacial and Holocene glacier fluctuations in North Island, New Zealand, Quaternary Sci. Rev., 223, 105914, https://doi.org/10.1016/j.quascirev.2019.105914, 2019.

Espanon, V. R., Honda, M., and Chivas, A. R.: Cosmogenic ^{3}He and ^{21}Ne surface exposure dating of young basalts from Southern Mendoza, Argentina, Quat. Geochronol., 19, 76–86, https://doi.org/10.1016/j.quageo.2013.09.002, 2014.

Fenton, C. R. and Niedermann, S.: Surface exposure dating of young basalts (1-200ka) in the San Francisco volcanic field (Arizona, USA) using cosmogenic ^{3}He and ^{21}Ne, Quat. Geochronol., 19, 87–105, https://doi.org/10.1016/j.quageo.2012.10.003, 2014.

Fenton, C. R., Webb, R. H., Pearthree, P. A., Cerling, T. E., and Poreda, R. J.: Displacement rates on the Toroweap and Hurricane faults: Implications for Quaternary downcutting in the Grand Canyon, Arizona, Geology, 29, 1035–1038, https://doi.org/10.1130/0091-7613(2001)029<1035:DROTTA>2.0.CO;2, 2001.

Fenton, C. R., Niedermann, S., Goethals, M. M., Schneider, B., and Wijbrans, J.: Evaluation of cosmogenic ^{3}He and ^{21}Ne production rates in olivine and pyroxene from two Pleistocene basalt flows, western Grand Canyon, AZ, USA, Quat. Geochronol., 4, 475–492, https://doi.org/10.1016/j.quageo.2009.08.002, 2009.

Ferrier, K. L., Taylor Perron, J., Mukhopadhyay, S., Rosener, M., Stock, J. D., Huppert, K. L., and Slosberg, M.: Covariation of climate and long-term erosion rates across a steep rainfall gradient on the Hawaiian island of Kaua'i, Bull. Geol. Soc. Am., 125, 1146–1163, https://doi.org/10.1130/B30726.1, 2013.

Fierstein, J., Hildreth, W., and Calvert, A. T.: Eruptive history of South Sister, Oregon Cascades, J. Volcanol. Geoth. Res., 207, 145–179, https://doi.org/10.1016/j.jvolgeores.2011.06.003, 2011.

Fleck, R. J., Hagstrum, J. T., Calvert, A. T., Evarts, R. C., and Conrey, R. M.: ^{40}Ar/^{39}Ar geochronology, paleomagnetism, and evolution of the Boring volcanic field, Oregon and Washington, USA, Geosphere, 1283–1314, https://doi.org/10.1130/GES00985.1, 2014.

Foeken, J. P., Day, S., and Stuart, F. M.: Cosmogenic ^{3}He exposure dating of the Quaternary basalts from Fogo, Cape Verdes: Implications for rift zone and magmatic reorganisation, Quat. Geochronol., 4, 37–49, https://doi.org/10.1016/j.quageo.2008.07.002, 2009.

Gabrielsen, H., Procter, J., Rainforth, H., Black, T., Harmsworth, G., and Pardo, N.: Reflections from an Indigenous Community on Volcanic Event Management, Communications and Resilience, in: Observing the Volcano World. Advances in Volcanology, edited by: Fearnley, C. J., Bird, D. K., Haynes, K., McGuire, W. J., and Jolly, G., Springer, Cham. 463–479, https://doi.org/10.1007/11157_2016_44, 2018.

Gallahan, W. E. and Nielsen, R. L.: The partitioning of Sc, Y, and the rare earth elements between high-Ca pyroxene and natural mafic to intermediate lavas at 1 atmosphere, Geochim. Cosmochim. Ac., 56, 2387–2404, https://doi.org/10.1016/0016-7037(92)90196-P, 1992.

Gamble, J. A., Price, R. C., Smith, I. E., McIntosh, W. C., and Dunbar, N. W.: ^{40}Ar/^{39}Ar geochronology of magmatic activity, magma flux and hazards at Ruapehu volcano, Taupo Volcanic Zone, New Zealand, J. Volcanol. Geoth. Res., 120, 271–287, https://doi.org/10.1016/S0377-0273(02)00407-9, 2003.

Gosse, J. C. and Phillips, F. M.: Terrestrial in situ cosmogenic nuclides: Theory and application, Quaternary Sci. Rev., 20, 1475–1560, https://doi.org/10.1016/S0277-3791(00)00171-2, 2001.

Greve, A., Turner, G. M., Conway, C. E., Townsend, D. B., Gamble, J. A., and Leonard, G. S.: Palaeomagnetic refinement of the eruption ages of Holocene lava flows, and implications for the eruptive history of the Tongariro Volcanic Centre, New Zealand, Geophys. J. Int., 207, 702–718, https://doi.org/10.1093/gji/ggw296, 2016.

Hackett, W. R.: Geology and petrology of Ruapehu volcano and related vents, PhD thesis, Victoria University of Wellington, http://researcharchive.vuw.ac.nz/handle/10063/743 (last access: 25 May 2024), 1985.

Harpel, C. J., Kyle, P. R., Esser, R. P., McIntosh, W. C., and Caldwell, D. A.: ^{40}Ar/^{39}Ar dating of the eruptive history of Mount Erebus, Antarctica: Summit flows, tephra, and caldera collapse, B. Volcanol., 66, 687–702, https://doi.org/10.1007/s00445-004-0349-7, 2004.

Harris, A. J. L.: Basaltic Lava Flow Hazard, in: Volcanic Hazards, Risks and Disasters, edited by: Shroder, J. F. and Papale, P., chap. 2, 17–46, Elsevier, https://doi.org/10.1016/C2011-0-07012-6, 2015.

Hilton, D. R., Fischer, T. P., and Marry, B.: Noble gases and volatile recycling at subduction zones, Rev. Mineral. Geochem., 47, 319–370, https://doi.org/10.2138/rmg.2002.47.9, 2002.

Houghton, B. F., Wilson, C. J., McWilliams, M. O., Lanphere, M. A., Weaver, S. D., Briggs, R. M., and Pringle, M. S.: Chronology and dynamics of a large silicic magmatic system: central Taupo Volcanic Zone, New Zealand, Geology, 23, 13–16, https://doi.org/10.1130/0091-7613(1995)023<0013:CADOAL>2.3.CO;2, 1995.

Jenkins, S. F., Day, S. J., Faria, B. V., and Fonseca, J. F.: Damage from lava flows: insights from the 2014–2015 eruption of Fogo, Cape Verde, Journal of Applied Volcanology, 6, 6, https://doi.org/10.1186/s13617-017-0057-6, 2017.

Keys, H. and Green, P. M.: Mitigation of volcanic risks at Mt Ruapehu, New Zealand, Proceedings of the Moutain Risks international conference, Firenze, Italy, 24–26 November, 485–490, https://www.researchgate.net/profile/Harry-Keys/publication/281606085_Mitigation_of_volcanic_risks_at_Mt_Ruapehu_New_Zealand/links/581f8fa608aeccc08af3abd6/Mitigation-of-volcanic-risks-at-Mt-Ruapehu-New-Zealand.pdf (last access: 25 May 2024), 2010.

Klein, J., Giegengack, R., Middleton, R., Sharma, P., Underwood, J. R., and Weeks, R. A.: Revealing Histories of Exposure Using in Situ Produced ^{26}Al and ^{10}Be in Libyian Desert Glass, Radiocarbon, 28, 547–555, 1986.

Kurz, M. D.: Cosmogenic helium in a terrestrial igneous rock, Nature, 320, 435–439, https://doi.org/10.1038/320435a0, 1986a.

Kurz, M. D.: In situ production of terrestrial cosmogenic helium and some applications to geochronology, Geochim. Cosmochim. Ac.,

50, 2855–2862, https://doi.org/10.1016/0016-7037(86)90232-2, 1986b.

Kurz, M. D., Colodner, D., Trull, T. W., Moore, R. B., and O'Brien, K.: Cosmic ray exposure dating with in situ produced cosmogenic ^{3}He: results from young Hawaiian lava flows, Earth Planet. Sc. Lett., 97, 177–189, https://doi.org/10.1016/0012-821X(90)90107-9, 1990.

Lal, D.: An important source of ^{4}He (and ^{3}He) in diamonds, Earth Planet. Sc. Lett., 96, 1–7, https://doi.org/10.1016/0012-821X(89)90118-0, 1989.

Lal, D.: Cosmic ray labeling of erosion surfaces: in situ nuclide production rates and erosion models, Earth Planet. Sc. Lett., 104, 424–439, https://doi.org/10.1016/0012-821X(91)90220-C, 1991.

Lanphere, M. A.: Comparison of conventional K-Ar and ^{40}Ar/^{39}Ar dating of young mafic volcanic rocks, Quaternary Res., 53, 294–301, https://doi.org/10.1006/qres.1999.2122, 2000.

Le Maitre, R. W.: Igneous Rocks: A Classification and Glossary of Terms, Recommendations of the International Union of Geological Sciences, Subcomission of the Systematics of Igneous Rocks, Cambridge University Press, https://doi.org/10.1017/CBO9780511535581, 2002.

Leonard, G. S., Cole, R. P. R., Christenson, B. W., Conway, C. E., Cronin, S. J., Gamble, J. A., Hurst, T., Kennedy, B. M., Miller, C. A., Procter, J. N., Pure, L. R., Townsend, D. B., White, J. D., and Wilson, C. J.: Ruapehu and Tongariro stratovolcanoes: a review of current understanding, New Zeal. J. Geol. Geop., 64, 389–420, https://doi.org/10.1080/00288306.2021.1909080, 2021.

Leya, I., Lange, H. J., Neumann, S., Wieler, R., and Michel, R.: The production of cosmogenic nuclides in stony meteoroids by galactic cosmic-ray particles, Meteorit. Planet. Sci., 35, 259–286, https://doi.org/10.1111/j.1945-5100.2000.tb01775.x, 2000.

Licciardi, J. M., Kurz, M. D., and Curtice, J. M.: Cosmogenic ^{3}He production rates from Holocene lava flows in Iceland, Earth Planet. Sc. Lett., 246, 251–264, https://doi.org/10.1016/j.epsl.2006.03.016, 2006.

Licciardi, J. M., Kurz, M. D., and Curtice, J. M.: Glacial and volcanic history of Icelandic table mountains from cosmogenic ^{3}He exposure ages, Quaternary Sci. Rev., 26, 1529–1546, https://doi.org/10.1016/j.quascirev.2007.02.016, 2007.

Lifton, N.: Implications of two Holocene time-dependent geomagnetic models for cosmogenic nuclide production rate scaling, Earth Planet. Sc. Lett., 433, 257–268, https://doi.org/10.1016/j.epsl.2015.11.006, 2016.

Lifton, N., Sato, T., and Dunai, T. J.: Scaling in situ cosmogenic nuclide production rates using analytical approximations to atmospheric cosmic-ray fluxes, Earth Planet. Sc. Lett., 386, 149–160, https://doi.org/10.1016/j.epsl.2013.10.052, 2014.

Lippolt, H. J. and Weigel, E.: ^{4}He diffusion in ^{40}Ar-retentive minerals, Geochim. Cosmochim. Ac., 52, 1449–1458, https://doi.org/10.1016/0016-7037(88)90215-3, 1988.

Lockwood, J. P. and Lipman, P. W.: Recovery of datable charcoal beneath young lavas: Lessons from Hawaii, Bulletin Volcanologique, 43, 609–615, https://doi.org/10.1007/BF02597697, 1980.

Luhr, J. F. and Carmichael, I. S. E.: The Colima Volcanic complex, Mexico, Contrib. Mineral. Petr., 71, 343–372, https://doi.org/10.1007/bf00374707, 1980.

Lupton, J. and Evans, L.: Changes in the atmospheric helium isotope ratio over the past 40 years, Geophys. Res. Lett., 40, 6271–6275, https://doi.org/10.1002/2013GL057681, 2013.

Marchetti, D. W., Hynek, S. A., and Cerling, T. E.: Cosmogenic ^{3}He exposure ages of basalt flows in the northwestern Payún Matru volcanic field, Mendoza Province, Argentina, Quat. Geochronol., 19, 67–75, https://doi.org/10.1016/j.quageo.2012.10.004, 2014.

Martin, L. C., Blard, P.-H., Balco, G., Lavé, J., Delunel, R., Lifton, N., and Laurent, V.: The CREp program and the ICE-D production rate calibration database: A fully parameterizable and updated online tool to compute cosmic-ray exposure ages, Quat. Geochronol., 38, 25–49, https://doi.org/10.1016/j.quageo.2016.11.006, 2017.

Matsuda, J., Matsumoto, T., Sumino, H., Nagao, K., Yamamoto, J., Miura, Y., Kaneoka, I., Takahata, N., and Sano, Y.: The ^{3}He/^{4}He ratio of new internal He Standard of Japan (HESJ), Geochem. J., 36, 191–195, https://doi.org/10.2343/geochemj.36.191, 2002.

Mc Arthur, J. L. and Shepherd, M. J.: Late Quaternary glaciation of Mt. Ruapehu, North Island, New Zealand, J. Roy. Soc. New Zeal., 20, 287–296, https://doi.org/10.1080/03036758.1990.10416823, 1990.

Medynski, S., Pik, R., Burnard, P., Vye-Brown, C., France, L., Schimmelpfennig, I., Whaler, K., Johnson, N., Benedetti, L., Ayelew, D., and Yirgu, G.: Stability of rift axis magma reservoirs: Spatial and temporal evolution of magma supply in the Dabbahu rift segment (Afar, Ethiopia) over the past 30 kyr, Earth Planet. Sc. Lett., 409, 278–289, https://doi.org/10.1016/j.epsl.2014.11.002, 2015.

Mishra, A. K., Placzek, C., Wurster, C., and Whitehead, P. W.: New radiocarbon age constraints for the 120 km-long Toomba flow, north Queensland, Australia, Aust. J. Earth Sci., 66, 71–79, https://doi.org/10.1080/08120099.2019.1523227, 2019.

Moore, R. B. and Rubin, M.: Radiocarbon dates for lava flows and pyroclastic deposits on Sao Miguel, Azores, Radiocarbon, 33, 151–164, https://doi.org/10.1017/S0033822200013278, 1991.

Morimoto, N., Fabries, J., Ferguson, A., Ginzburg, I., Ross, M., Seifert, F., Zussman, J., Aoki, K., and Gottardi, G.: Nomenclature of pyroxenes Subcommittee on Pyroxenes Commission on New Minerals and Mineral Names International Mineralogical Association, Am. Mineral., 73, 1123–1133, 1988.

Muscheler, R., Beer, J., Kubik, P. W., and Synal, H. A.: Geomagnetic field intensity during the last 60,000 years based on ^{10}Be and ^{36}Cl from the Summit ice cores and ^{14}C, Quaternary Sci. Rev., 24, 1849–1860, https://doi.org/10.1016/j.quascirev.2005.01.012, 2005.

Nairn, I. A., Kobayashi, T., and Nakagawa, M.: The ∼ 10 ka multiple vent pyroclastic eruption sequence at Tongariro Volcanic Centre, Taupo Volcanic Zone, New Zealand: Part 1. Eruptive processes during regional extension, J. Volcanol. Geoth. Res., 86, 19–44, https://doi.org/10.1016/S0377-0273(98)00085-7, 1998.

Nicholls, I. A. and Harris, K. L.: Experimental rare earth element partition coefficients for garnet, clinopyroxene and amphibole coexisting with andesitic and basaltic liquids, Geochim. Cosmochim. Ac., 44, 287–308, https://doi.org/10.1016/0016-7037(80)90138-6, 1980.

Niedermann, S.: Cosmic-ray-produced noble gases in terrestrial rocks: Dating tools for surface processes, Rev. Mineral. Geochem., 47, 731–784, https://doi.org/10.2138/rmg.2002.47.16, 2002.

Nishiizumi, K.: Cosmic ray production rates of ^{10}Be and ^{26}Al in quartz from glacially polished rocks, J. Geophys. Res., 94, 17907–17915, https://doi.org/10.1029/jb094ib12p17907, 1989.

Nishiizumi, K., Kohl, C. P., Arnold, J. R., Klein, J., Fink, D., and Middleton, R.: Cosmic ray produced ^{10}Be and ^{26}Al in Antarctic rocks: exposure and erosion history, Earth Planet. Sc. Lett., 104, 440–454, https://doi.org/10.1016/0012-821X(91)90221-3, 1991.

Palmer, B. A. and Neall, V. E.: The Murimotu Formation – 9500 year old deposits of a debris avalanche and associated lahars, Mount Ruapehu, North Island, New Zealand, New Zeal. J. Geol. Geop., 32, 477–486, https://doi.org/10.1080/00288306.1989.10427555, 1989.

Pardo, N.: Andesitic Plinian Eruptions at Mt. Ruapehu (New Zealand): From Lithofacies to Eruption Dynamics, PhD thesis, Massey University, https://mro.massey.ac.nz/items/c2f61b33-2579-410f-b493-eeab08691375 (last access: 25 May 2024), 2012.

Pardo, N., Cronin, S., Palmer, A., Procter, J., and Smith, I.: Andesitic Plinian eruptions at Mt. Ruapehu: Quantifying the uppermost limits of eruptive parameters, B. Volcanol., 74, 1161–1185, https://doi.org/10.1007/s00445-012-0588-y, 2012a.

Pardo, N., Cronin, S. J., Palmer, A. S., and Németh, K.: Reconstructing the largest explosive eruptions of Mt. Ruapehu, New Zealand: Lithostratigraphic tools to understand subplinian-plinian eruptions at andesitic volcanoes, B. Volcanol., 74, 617–640, https://doi.org/10.1007/s00445-011-0555-z, 2012b.

Parmelee, D. E., Kyle, P. R., Kurz, M. D., Marrero, S. M., and Phillips, F. M.: A new Holocene eruptive history of Erebus volcano, Antarctica using cosmogenic ^{3}He and ^{36}Cl exposure ages, Quat. Geochronol., 30, 114–131, https://doi.org/10.1016/j.quageo.2015.09.001, 2015.

Patterson, D. B., Honda, M., and McDougall, I.: Noble gases in mafic phenocrysts and xenoliths from New Zealand, Geochim. Cosmochim. Ac., 58, 4411–4427, https://doi.org/10.1016/0016-7037(94)90344-1, 1994.

Preece, K., Mark, D. F., Barclay, J., Cohen, B. E., Chamberlain, K. J., Jowitt, C., Vye-Brown, C., Brown, R. J., and Hamilton, S.: Bridging the gap: ^{40}Ar/^{39}Ar dating of volcanic eruptions from the "Age of Discovery", Geology, 46, 1035–1038, https://doi.org/10.1130/G45415.1, 2018.

Price, R. C., Gamble, J. A., Smith, I. E., Maas, R., Waight, T., Stewart, R. B., and Woodhead, J.: The anatomy of an andesite volcano: A time-stratigraphic study of andesite petrogenesis and crustal evolution at Ruapehu Volcano, New Zealand, J. Petrol., 53, 2139–2189, https://doi.org/10.1093/petrology/egs050, 2012.

Puchol, N., Blard, P.-H., Pik, R., Tibari, B., and Lavé, J.: Variability of magmatic and cosmogenic ^{3}He in Ethiopian river sands of detrital pyroxenes: Impact on denudation rate determinations, Chem. Geol., 448, 13–25, https://doi.org/10.1016/j.chemgeo.2016.10.033, 2017.

Pure, L. R., Leonard, G. S., Townsend, D. B., Wilson, C. J., Calvert, A. T., Cole, R. P., Conway, C. E., Gamble, J. A., and Smith, T. B.: A high resolution ^{40}Ar/^{39}Ar lava chronology and edifice construction history for Tongariro volcano, New Zealand, J. Volcanol. Geoth. Res., 403, 106993, https://doi.org/10.1016/j.jvolgeores.2020.106993, 2020.

Ramos, F. C., Heizler, M. T., Buettner, J. E., Gill, J. B., Wei, H. Q., Dimond, C. A., and Scott, S. R.: U-series and ^{40}Ar/^{39}Ar ages of Holocene volcanic rocks at Changbaishan volcano, China, Geology, 44, 511–514, https://doi.org/10.1130/G37837.1, 2016.

Rhodes, E.: The Draining of an Andesitic Valley-Confined Lava Flow, Mt Ruapehu, Honours thesis, University of Canterbury, 2012.

Schaefer, J. M., Winckler, G., Blard, P.-H., Balco, G., Shuster, D. L., Friedrich, R., Jull, A. J. T., Wieler, R., and Schluechter, C.: Performance of CRONUS-P – A pyroxene reference material for helium isotope analysis, Quat. Geochronol., 31, 237–239, https://doi.org/10.1016/j.quageo.2014.07.006, 2016.

Schimmelpfennig, I., Williams, A., Pik, R., Burnard, P., Niedermann, S., Finkel, R., Schneider, B., and Benedetti, L.: Intercomparison of cosmogenic in-situ ^{3}He, ^{21}Ne and ^{36}Cl at low latitude along an altitude transect on the SE slope of Kilimanjaro volcano (3° S, Tanzania), Quat. Geochronol., 6, 425–436, https://doi.org/10.1016/j.quageo.2011.05.002, 2011.

Sherrod, D. R., Hagstrum, J. T., Mcgeehin, J. P., Champion, D. E., and Trusdell, F. A.: Distribution , ^{14}C chronology , and paleomagnetism of latest Pleistocene and Holocene lava flows at Haleakala Island of Maui , Hawai'i: A revision of lava flow hazard zones, J. Geophys. Res., 111, B05205, https://doi.org/10.1029/2005JB003876, 2006.

Shuster, D. L., Farley, K. A., Sisterson, J. M., and Burnett, D. S.: Quantifying the diffusion kinetics and spatial distributions of radiogenic ^{4}He in minerals containing proton-induced ^{3}He, Earth Planet. Sc. Lett., 217, 19–32, https://doi.org/10.1016/S0012-821X(03)00594-6, 2004.

Smith, J. A., Finkel, R. C., Farber, D. L., Rodbell, D. T., and Seltzer, G. O.: Moraine preservation and boulder erosion in the tropical Andes: Interpreting old surface exposure ages in glaciated valleys, J. Quaternary Sci., 20, 735–758, https://doi.org/10.1002/jqs.981, 2005.

Stipp, J.: The Geochronology and Petrogenesis of the Cenozoic Volcanics of the North Island, New Zealand, PhD thesis, Australian National University, https://www.proquest.com/docview/2617247792?pq-origsite=gscholar&fromopenview=true&sourcetype=Dissertations&Theses (last access: 9 July 2023), 1968.

Stone, J. O.: Air pressure and cosmogenic isotope production, J. Geophys. Res.,, 105, 753–759, https://doi.org/10.1029/2000JB900181, 2000.

Tanaka, H., Kawamura, K., Nagao, K., and Houghton, B. F.: K-Ar ages and paleosecular variation of direction and intensity from quaternary lava sequences in the Ruapehu Volcano, New Zealand, Earth Planets Space, 49, 587–599, https://doi.org/10.5636/jgg.49.587, 1997.

Topping, W. W.: Some aspects of quaternary history of Tongariro Volcanic Centre, PhD thesis, Victoria University of Wellington, https://openaccess.wgtn.ac.nz/articles/thesis/Some_Aspects_of_Quaternary_History_of_Tongariro_Volcanic_Centre/19252133/1 (last access: 9 July 2023) 1974.

Topping, W. W. and Kohn, B. P.: Rhyolitic tephra marker beds in the Tongariro area, North Island, New Zealand, New Zeal. J. Geol. Geop., 16, 375–395, https://doi.org/10.1080/00288306.1973.10431367, 1973.

Townsend, D., Leonard, G., Conway, C., Eaves, S., and Wilson, C.: Geology of the Tongariro National Park Area, GNS Science, pp. 1 sheet + 109 pp., ISBN 978-1-98-853030-7, 2017.

Tremblay, M. M., Shuster, D. L., and Balco, G.: Diffusion kinetics of ^{3}He and ^{21}Ne in quartz and implications for cosmogenic noble gas paleothermometry, Geochim. Cosmochim. Ac., 142, 186–204, https://doi.org/10.1016/j.gca.2014.08.010, 2014.

Trusdell, F. A.: Lava flow hazards and risk assessment on Mauna Loa Volcano, Hawaii, Geoph. Monog. Series, 92, 327–336, https://doi.org/10.1029/GM092p0327, 1995.

Tsang, S. and Lindsay, J.: Lava flow crises in inhabited areas part I: Lessons learned and research gaps related to effusive, basaltic eruptions, Journal of Applied Volcanology, 9, 9, https://doi.org/10.1186/s13617-020-00096-y, 2020.

Turner, G. M. and Corkill, R. M.: NZPSV11k.2023 and NZPSV1k.2023: Holocene palaeomagnetic secular variation master records for New Zealand, Phys. Earth Planet. In., 344, 107093, https://doi.org/10.1016/j.pepi.2023.107093, 2023.

Turner, G. M., Howarth, J. D., de Gelder, G. I., and Fitzsimons, S. J.: A new high-resolution record of Holocene geomagnetic secular variation from New Zealand, Earth Planet. Sc. Lett., 430, 296–307, https://doi.org/10.1016/j.epsl.2015.08.021, 2015.

Uppala, S. M., Kållberg, P. W., Simmons, A. J., Andrae, U., da Costa Bechtold, V., Fiorino, M., Gibson, J. K., Haseler, J., Hernandez, A., Kelly, G. A., Li, X., Onogi, K., Saarinen, S., Sokka, N., Allan, R. P., Andersson, E., Arpe, K., Balmaseda, M. A., Beljaars, A. C., van de Berg, L., Bidlot, J., Bormann, N., Caires, S., Chevallier, F., Dethof, A., Dragosavac, M., Fisher, M., Fuentes, M., Hagemann, S., Hólm, E., Hoskins, B. J., Isaksen, L., Janssen, P. A., Jenne, R., McNally, A. P., Mahfouf, J. F., Morcrette, J. J., Rayner, N. A., Saunders, R. W., Simon, P., Sterl, A., Trenberth, K. E., Untch, A., Vasiljevic, D., Viterbo, P., and Woollen, J.: The ERA-40 re-analysis, Q. J. Roy. Meteor. Soc., 131, 2961–3012, https://doi.org/10.1256/qj.04.176, 2005.

Vermeesch, P.: IsoplotR: A free and open toolbox for geochronology, Geosci. Front., 9, 1479–1493, https://doi.org/10.1016/j.gsf.2018.04.001, 2018.

Villemant, B.: Trace element evolution in the Phlegrean Fields (Central Italy): fractional crystallization and selective enrichment, Contrib. Mineral. Petr., 98, 169–183, https://doi.org/10.1007/BF00402110, 1988.

Wijbrans, J., Schneider, B., Kuiper, K., Calvari, S., Branca, S., De Beni, E., Norini, G., Corsaro, R. A., and Miraglia, L.: ^{40}Ar/^{39}Ar geochronology of Holocene basalts; examples from Stromboli, Italy, Quat. Geochronol., 6, 223–232, https://doi.org/10.1016/j.quageo.2010.10.003, 2011.

Wilson, C. J., Gravley, D. M., Leonard, G. S., and Rowland, J. V.: Volcanism in the central Taupo Volcanic Zone, New Zealand: tempo, styles and controls, in: Studies in Volcanology: The Legacy of George Walker, edited by: Thordarson, T., Special Publications of IAVCEI 2, 225–247, https://doi.org/10.1144/IAVCEl002.12, 2009.

Wilson, G., Wilson, T. M., Deligne, N. I., and Cole, J. W.: Volcanic hazard impacts to critical infrastructure: A review, J. Volcanol. Geoth. Res., 286, 148–182, https://doi.org/10.1016/j.jvolgeores.2014.08.030, 2014.

Wright, H. M., Vazquez, J. A., Champion, D. E., Calvert, A. T., Mangan, M. T., Stelten, M., Cooper, K. M., Herzig, C., and Jr, A. S.: Episodic Holocene eruption of the Salton Buttes rhyolites, California, from paleomagnetic, U-Th, and Ar/Ar dating Heather, Geochem., Geophy. Geosy., 16, 1198–1210, https://doi.org/10.1002/2015GC005714, 2015.

Zimmermann, L., Avice, G., Blard, P.-H., Marty, B., Füri, E., and Burnard, P. G.: A new all-metal induction furnace for noble gas extraction, Chem. Geol., 480, 86–92, https://doi.org/10.1016/j.chemgeo.2017.09.018, 2018.